Università degli Studi di Padova
Dipartimento di Ingegneria Industriale

Laurea Magistrale in Ingegneria Elettrica

Rotary Transformer Design for Brushless Electrically Excited Synchronous Machines

in collaborazione con Technische Universität München
presso Fachgebiet Energiewandlungstechnik

Candidato:
Mattia Tosi

Relatore:
Ch.mo Prof. Nicola Bianchi

Correlatori:
Prof. Dr.-Ing. Hans-Georg Herzog
Dipl.-Ing. Jörg Kammermann

Anno Accademico 2013 - 2014

Ai miei genitori e alla mia famiglia,
perché mi hanno sempre sostenuto in questi anni di studio.

Sommario

Negli ultimi tempi, viene sempre più valutata la possibilità di sostituire i motori sincroni a magneti permanenti con i tradizionali motori sincroni a rotore avvolto per la trazione elettrica stradale. Infatti, nonostante l'elevato rendimento dei motori a magneti permanenti, assieme all'alta densità di potenza e alla grande affidabilità, l'utilizzo dei magneti permanenti a terre rare comporta svantaggi economici e problemi di inquinamento.

Il principale svantaggio dei motori sincroni tradizionali per un loro utilizzo nella trazione elettrica consiste nella presenza ingombrante del sistema di eccitazione a spazzole-collettore. In questa tesi, si propone la sostituzione di tale sistema con un trasformatore rotante. Tramite un trasferimento di energia *contactless*, si eviterebbe quindi la manutenzione delle spazzole, riducendo anche gli spazi occupati.

Un trasformatore rotante è un trasformatore assialsimmetrico con traferro, il quale permette la rotazione relativa tra primario e secondario. Il secondario è calettato sull'albero del rotore. La presenza del traferro comporta valori non usuali delle induttanze.

Le induttanze di dispersione e di magnetizzazione sono state analizzate analiticamente prima dello stadio di design. Vengono analizzate due geometrie: *pot core* e *axial*. I trasformatori vengono preliminarmente progettati grazie a un algoritmo di ottimizzazione, e successivamente analizzati e confrontati con un software agli elementi finiti. Per la particolare applicazione di questo lavoro, la geometria *pot core* sembra più adatta. Il trasformatore rotante risulta inoltre meno ingombrante del sistema spazzole-collettore.

In conclusione, il motore sincrono a rotore avvolto con trasformatore rotante risulta complessivamente meno efficiente del motore a magneti permanenti. Infatti, sebbene il trasformatore preso singolarmente sia più prestante del collettore, il complesso trasformatore-convertitore elettronico ha un'efficienza decisamente minore. Le perdite sono principalmente di conduzione e commutazione nell'elettronica, a causa delle elevate correnti primarie legate a un basso valore dell'induttanza di magnetizzazione. É comunque possibile migliorare ulteriormente il sistema, ad esempio utilizzando ove possibile tecniche di *soft switching* per il convertitore.

Abstract

Lately, for automotive applications, it seems profitable to substitute the Permanent Magnets Synchronous Motor with the traditional Electrically Excited Synchronous Machine. In fact, despite the remarkable efficiency of the permanent magnets, and despite their compactness and reliability, there are economical and environmental issues related to the use of rare earth magnets inside electrical machines.

The most demanding problems with the implementation of the Electrically Excited Synchronous Motors inside a vehicle, are due to the cumbersome presence of the brushes and slip rings system for the rotor's excitation. In this thesis, the possibilities to replace this system with a rotary transformer are investigated, in order to achieve a contact-less energy transfer, avoiding thus also the wear of the brushes.

A rotary transformer is a transformer with an axial symmetry, with an air gap between the primary side and the secondary side that allows the rotation of the latter. The secondary side is keyed onto the rotor's shaft. The inherent air gap leads to a non-conventional behavior of the transformer, in particular regarding the inductances. The leakage inductance and the main inductance are analyzed analytically before the design. The geometries of two typologies of rotary transformer are found through an optimization algorithm: the pot core and the axial rotary transformers. The optimized geometries are then analyzed and compared with a Finite Element Analysis software. For the studied application, the pot core rotary transformer seems more suitable, and it is also less bulky than the brushes and slip rings system.

From this work, it results that the Electrically Excited Synchronous Motor with a rotary transformer is not competitive in terms of efficiency with a Permanent Magnets Synchronous Motor, unless the efficiency of the whole rotary transformer's excitation system does not improve. In fact, although the efficiency of the transformers themselves is better than the brushes and slip rings', a relatively big leakage inductance and a small main inductance cause considerable losses in the electronic converter, thus resulting in an overall low efficiency. However, this technology is not yet very experienced and there is still room for improvement; it is indeed possible to reduce the overall losses with a soft switching technique on the electronics, or it is possible to improve the cooling of rotating parts.

Contents

CHAPTER 1

Introduction

Nowadays, there are many different typologies of electric motors that can be used for the traction of a fully electric road vehicle. Even though an electric motor can be more or less complex and it can have different characteristics, for automotive applications there are some features that are always demanded. The electric drive in a vehicle should be light and compact and it must have a good efficiency; in brief it should have a high power density. For mass produced machines, the cost achieves a greater importance and it must be as low as possible. Lastly, the torque and speed characteristic has a defined trait, as it is shown in fig. 1.1. Talking about automotive applications, the torque for low speeds must be high but constant, for great accelerations and comfort, while with the increase of the speed, the torque decreases with a constant power output.
The most commonly used motors are: the asynchronous motor (ASM), the permanent magnet synchronous motor (PMSM) with superficial magnets or internal magnets, and the traditional electrically excited synchronous motor (EESM).

Regarding the desired features for the electric traction, every one of these machine has upsides and downsides. The ASM has a simple structure, its cost is low and it does not use permanent magnets (PM); on the other hand, it has a relatively low efficiency, and its torque-speed characteristic is far from ideal. The PMSM is nowadays the most used motor for automotive applications. In fact, it has a high efficiency combined with extreme compactness, and the mechanical characteristic is almost ideal, with low torques for a wide range of speeds. The drawbacks are all linked to the presence of PM: its cost is high and it depends on the market's value of the magnets. Furthermore, the PM have environmental issues. At last, the EESM has a good efficiency, the mechanical characteristic is similar to the

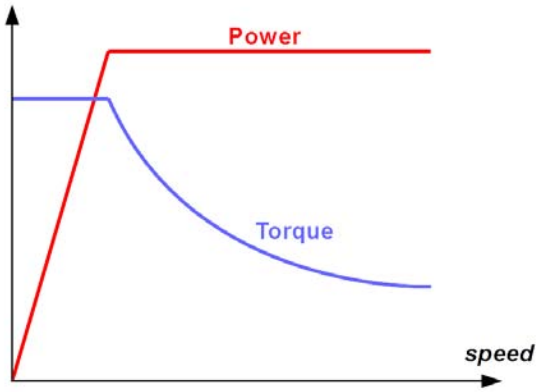

Figure 1.1: Qualitative ideal torque-speed characteristic.

ideal and, with an adequate regulation of the current on the rotor, the possibilities of regulation and control are multiplied and we would be able to optimize the efficiency and the mechanical characteristic for every working condition [11]. Furthermore, the EESM does not have PM. Unfortunately, the current on the rotor is also a drawback: it causes resistive losses on the rotor, where it is difficult to do an effective cooling.

This thesis comes from the desire to avoid permanent magnets inside the electrical machines. In fact, permanent magnets have two main problems: monopoly of the sources and environmental impact. The most used permanent magnets used for automotive applications come from *rare earth elements*: for instance samarium-cobalt and neodymium-iron-boron. The 90% of the global provision of rare earth metals is in China, even if only the 23% are proven reserves [2]. Only the Bayan Obo Mining District in the Inner Mongolia, counts the 45% of the global production of rare earth metals [1]. During the last years, China has announced restrictions on the production and on the export of this materials, causing a sudden increase in the rare earths' cost. Recently, they have been discovered many others countries with rare earth deposits, and the price of the PM is almost stable [20]. Nonetheless, the environmental problems are still present. There are often radioactive materials mixed with the rare earths, and during the refining process toxic acids are used. For these reasons, many manufacturers are trying to avoid the utilization of these materials.

The Institute of Energy Conversion Technology at the Department of Electrical Engineering and Information Technology of the Technische Universität München, worked on an EESM for automotive applications with high performances. But they encountered another drawback of the EESM: the size. In fact, due to the presence of the rotor excitation, a brushes and slip rings system is present. This kind of electromechanical device has many disadvantages: it is bulky, the brushes

make dust and need maintenance, decreasing thus the reliability of the whole motor.

The proposed solution of this thesis is to replace the brushes and slip rings system with a *rotary transformer*, in order to excite the rotor of the same EESM. A rotary transformer is a transformer with an axial symmetry and an air gap between the primary side and the secondary side, accordingly allowing the rotation of one of the two parts. The aim is to achieve contact-less energy transfer, avoiding the wear of the rotating parts, and hopefully reducing the space occupied.

Structure of the Thesis

In this thesis it is studied a particular application for a rotary transformer, but the aim is to give a general overview on the rotary transformer's behavior in order to give the possibility to design a rotary transformer also for different applications.

The structure of the work that is done in this thesis is the following.

- At the beginning, there is a brief description of the state of the art for the rotary transformers.
- After that, there is an introduction to the specific case that is considered, followed by the choice of the converters that can be used for the rotor's excitation with a rotary transformer.
- Before the design, there is an analytical modeling of the transformers. This is important for the design in order to understand the problems that are behind the rotary transformer.
- The design, because of the small literature and because in the specific case there are geometrical limitations, is done through an optimization algorithm.
- With the optimized geometry there are some Finite Element Analysis simulations. Thanks to these, it is possible to find a working (or more than one) rotary transformer, and to see then the degrees of freedom in the design process.
- Finally, it is done a comparison between two kinds of rotary transformers and it is chosen the best one for the specific application.

CHAPTER 2

Rotary Transformer Technology

The rotary transformer is a single-phase transformer with an axial symmetry and an air gap between the primary side and the secondary side. The air gap allows the rotation of one half of the core, without influencing the flux lines and the inductive power transfer between the primary and secondary side.

There are different typologies of rotary transformers [22]. The shape of the magnetic core can change, as well as the relative position of the windings and their collocation inside the slots [14].

The two typologies considered in this work are the *pot core* and the *axial* rotary transformers, left and right in fig. 2.1. Both transformers have the secondary side

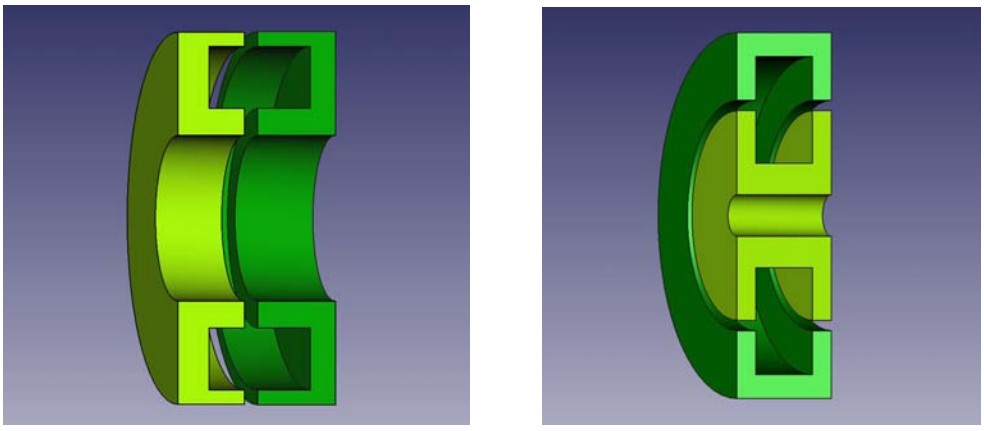

(a) Pot core. (b) Axial.

Figure 2.1: 3D section of two rotary transformers.

(in light green) keyed on a shaft; the primary side (dark green) is kept still and it is connected to the power supply. The secondary side powers the rotating load, in our case the excitation winding of a synchronous machine.

The coils are wrapped around the magnetic core, but they can be placed inside the slots in different ways. The windings can be *adjacent* or *coaxial*.

In fig. 2.2, it is shown an adjacent winding. It is the most common and easy way to place the coils, because the air gap is completely free and it can be really small.

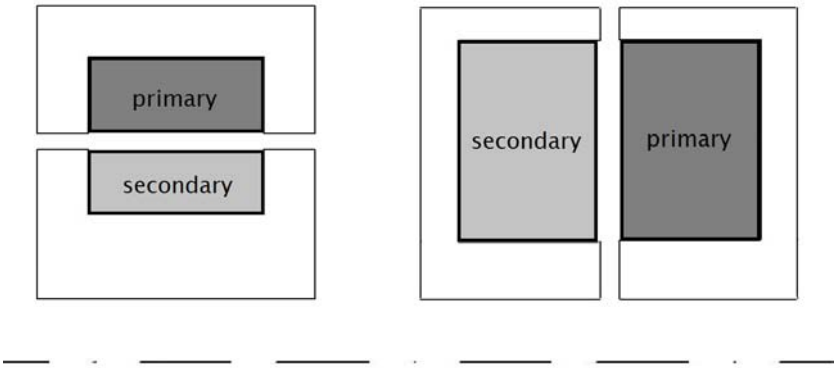

Figure 2.2: Adjacent windings for axial (left) and pot core (right).

In fig. 2.3, there are the coaxial windings. They allow a better magnetic coupling with a lower value of leakage inductance, but it is difficult to place the coils, above all if there is a small air gap.

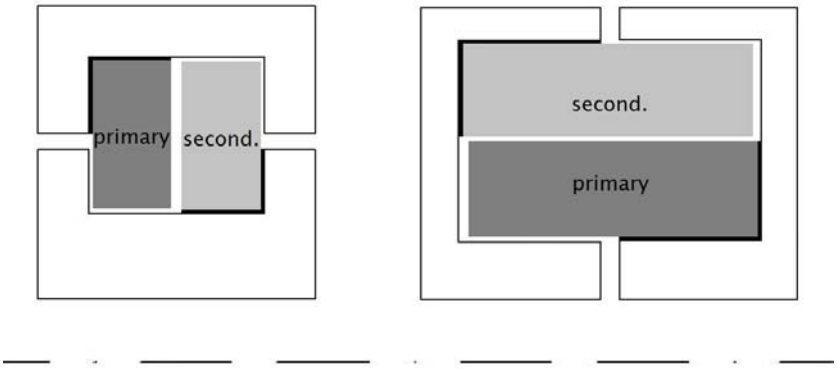

Figure 2.3: Coaxial windings for axial (left) and pot core (right).

In our case, we have a very small machine, and so a small air gap, with a high rotational speed. It is then advised to use the adjacent configuration.

2.1. Effects of the air gap

Although the air gap is mandatory in order to have the rotation, it influences deeply the electromagnetic behavior of the rotary transformer [18].

The main effects of the air gap can be traced to two fundamental characteristics of a transformer: the *main inductance*, L_m, and the *leakage inductance*, L_{lk}.

Main inductance In general, the air gap leads to a low coupling coefficient for the transformer. This means that a part of the total supplied energy is stored inside the transformer's body, in particular into the air gap, because of the magnetic permeability of the air respect to the high permeability of the magnetic core.

Consequently, the main inductance of a rotary transformer is much lower than the one of a normal transformer; and it can be compared with its leakage inductance.

Accordingly then, there is a high magnetizing current, and the primary coils have to sustain an high primary current, plus the secondary reflected current. This leads to high resistive losses on the primary side, with problems in the power electronics and in the cooling system.

Leakage inductance The physical separation between primary side and secondary side, causes a high leakage inductance. In fact, the leakage inductance is connected to the lost magnetic flux: with the air gap there are different paths available for the magnetic flux and so more losses.

The leakage inductance then, is in series with the transformer and can:

- store the high primary current and release it causing problem with the power electronics;
- cause a voltage drop not negligible on the primary side.

This last point means an impaired voltage gain.

2.2. Implementation in a power system

There is a big difference in the hardware's architecture of the whole power system. If we are talking about an automotive application, the power supply will be a battery. So, with a DC voltage source, the conventional architecture of the whole system is composed by the main inverter, which feeds the three-phase winding of the stator, and, if it is an electrically excited synchronous motor, it is necessary a converter that controls the current that goes to the rotor winding, through the slip rings system. If the motor is an asynchronous motor, or a permanent magnet (PM)

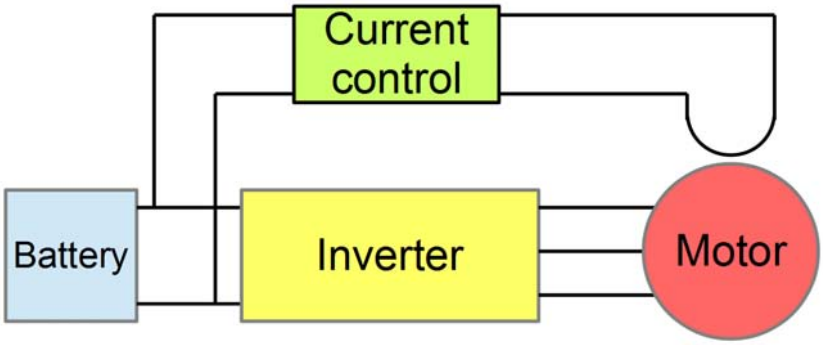

Figure 2.4: Conventional architecture for an electrically excited synchronous motor [10].

synchronous motor, there is only the main inverter.

With the rotary transformer, it is needed more hardware. In fact a transformer needs an AC voltage, so there must be an inverter and a rectifier (see fig. 2.5). But we can see there the main advantage of a rotary transformer, and, in general,

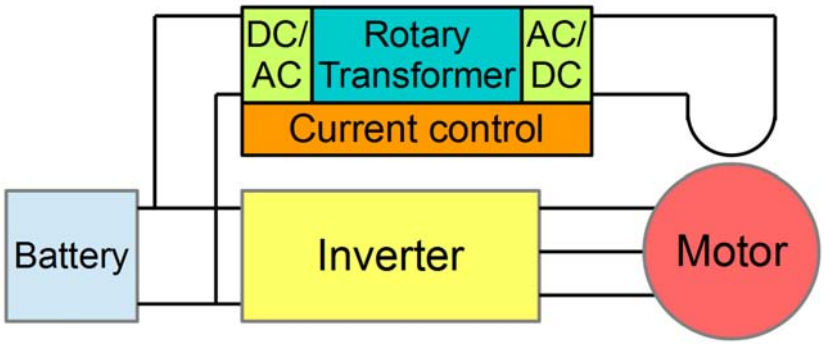

Figure 2.5: Architecture for an electrically excited synchronous motor with the rotary transformer [12] [11].

of an electrically excited synchronous machine. For an asynchronous motor, the main advantage is the easy structure and the low cost, but the power factor is low, and the power curve is not really suitable for automotive applications because the power decreases with the speed. The permanent magnet motors, have a high efficiency, a high power density, combined with a very good power-torque curve, but they use permanent magnets. The electrically excited ones, finally, have the same power curve of the PM, a good power factor, and, despite the additional losses in the rotor windings, they can have a current regulation on the rotor side, resulting in an optimized efficiency along the power-torque characteristic.

Having said that, in our case we need an additional converter to make the

rotary transformer work. For this kind of application it seems advantageous to use a dc-dc converter with Galvanic isolation. This converters have a dc input and a dc output, and the galvanic separation is done through a transformer. The fact that, in this case, the transformer rotates, does not change the operation of the converter.

These kind of converters all work in the same way: the dc source is made ac at the transformer's input terminals and the ac output of the transformer is then rectified. We have only to pay attention to the fact that the rectifier will rotate.

Usually then, the output is filtered through a L-C branch. For this particular application, the inductive part of this filter could be made by the inductive component of the rotor windings.

Typical dc-dc converters with Galvanic isolation, suitable for our application, are [17]:

- the forward,
- the half-bridge,
- the full-bridge.

We choose the full-bridge for many reasons. The cross sectional area of a transformer's core has the following expression (see subsection 4.2.2):

$$A_c = \frac{V_{in} \cdot D}{2 \cdot N_1 \cdot f \cdot \Delta B_{max}} \tag{2.1}$$

where D is the duty cycle, N_1 the primary coils of the transformer, f the switching frequency, and ΔB_{max} is the value of the flux density from zero to its maximal value during a period of the hysteresis cycle. This period is the same as the period $T = 1/f$.

If we want a small transformer, and so a small A_c, the ΔB_{max} must be as high as possible.

- The forward converter has a continuous component of the current, and of the magnetic flux, on the transformer's coils (uni-directional excitation). Consequently, $\Delta B_{max} < (1/2)(B_{sat} - B_{res})$. The full-bridge has a bi-directional excitation, and no continuous component of the flux in a period. This means that $\Delta B_{max} < B_{sat}$, so more flux density available, and the possibility to do a smaller core.
- The current in the half-bridge switches is the double of the current in the full-bridge ones. The full-bridge is more suitable for high power applications ($> 1\ kW$) and applications with high primary currents.
- With the full-bridge there is the possibility of the *Zero Voltage Transition* (ZVT) [13], that allows zero voltage switching, thus reducing the commutation losses in the converter.

CHAPTER 3

The whole power system

In this work, we will study the design of a suitable rotary transformer in order to give the rotor excitation of a synchronous machine, thus replacing the slip rings system. With the aim of simplifying the comprehension of the many factors that affect a rotary transformer's behavior, we want here to excite the rotor of an existing synchronous motor.

The motor in question is called *ELANi Machine*, and it is a motor developed by the Technische Universität München, in Munich, Germany. It is a three-phase electrically excited synchronous motor for e-scooters, with a power of 12 kW.

The peculiar characteristic of the *ELANi Machine* is its size. In fact, because of the very narrow spaces inside a scooter's carter, the volume of the motor system must be particularly limited. If we take the whole machine system, thus motor, power electronics, and cooling system, it must be all inside a virtual cubic box of side 180 mm. Because of a misunderstanding between industries and university, the designed *ELANi Machine* is too long. As it is shown in fig. 3.1, the transversal dimensions of the machine are inside the limits, but the length is too big. In fact, it comprehends, as well as the motor itself, also the power electronics and the slip rings system.

Since the power electronics' volume seems to be already optimized, a good chance to reduce the axial length of the propulsion system is to replace the bulky slip rings apparatus with a rotary transformer. Therefore, the volume of the transformer will be a significant criterion during the design.

There are two possible versions of the *ELANi Machine*; one with 4 salient poles on the rotor, and the other one with 6 poles. The version considered in this work is the four pole *ELANi Machine*.

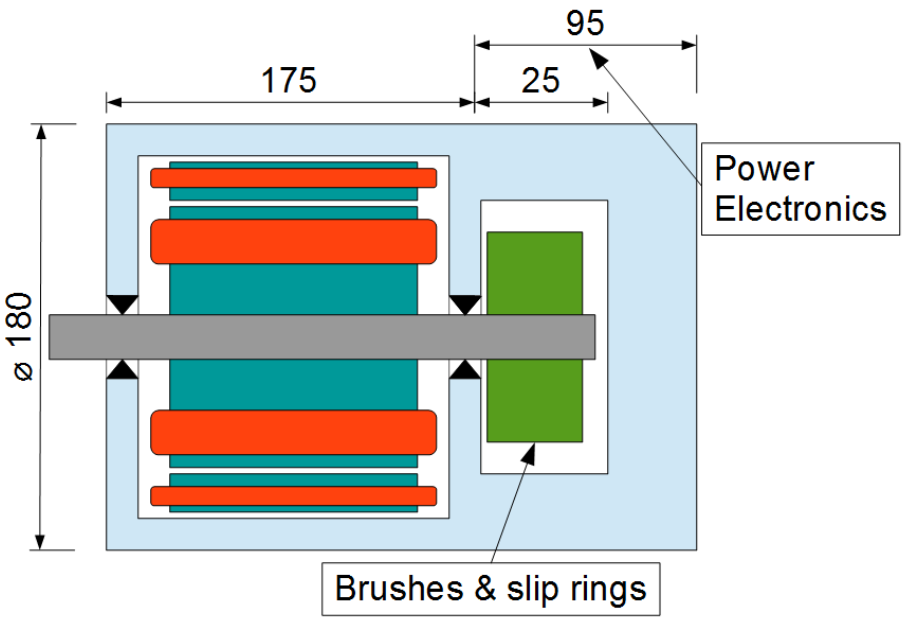

Figure 3.1: Qualitative side view of the ELANi Machine.

Since the project has not gone beyond the first stage of the design, there is only a finite element analysis simulation available. For this reason, many characteristics (physical, electromagnetic, and geometrical) of the motor are not defined. Therefore, we will respect only the features of the machine that are given; the quantities not known are here arbitrarily estimated, as we can see in the following pages.

Anyhow, this is not a great issue. This thesis aims to illustrate a general procedure to design a rotary transformer, so that the design process shown here can be replicated for other particular projects.

3.1. Requirements for the rotor's excitation

The four poles *ELANi Machine* has a rated torque of 30.8 Nm at the rated speed of 4000 rpm; beyond this speed, the torque decreases hyperbolically along the mechanical characteristic, with a constant rated power of 12 kW, up to the maximum speed of 12000 rpm.

In order to achieve the rated torque of 30.8 Nm during the constant torque phase, we need 1900 Ampere-turns per pole, so a total of 7600 A for the whole rotor excitation; in fact the four poles are series-connected. The area available for the winding A_{Cu} for each pole of the machine, shown in fig. 3.2 (the orange or the blue part), corresponds to 200 mm^2. The current densities set for the conductors

are 12 $\frac{\text{A}}{\text{mm}^2}$ for the stator and 10 $\frac{\text{A}}{\text{mm}^2}$ for the rotor.

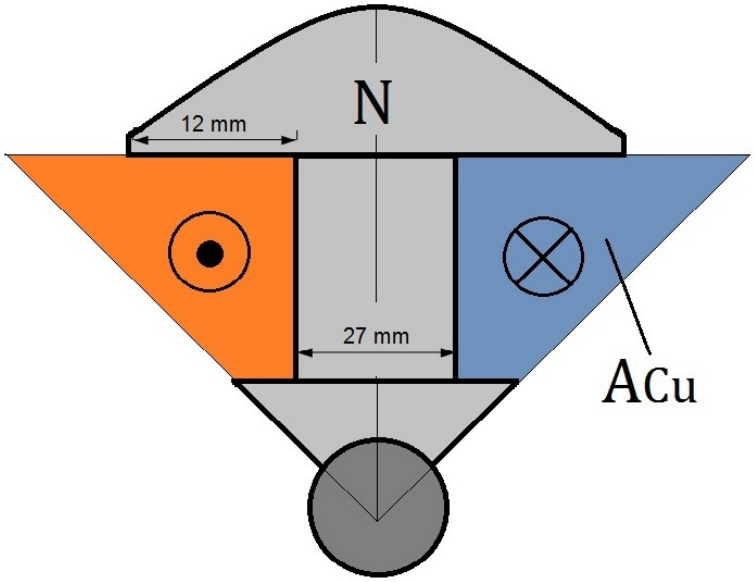

Figure 3.2: North pole of the *ELANi Machine* (qualitative, not in scale).

Now, our aim is to calculate the current and the voltage that are needed at the rotor winding terminals, in order to achieve the Ampere-turns per pole value of 1900 A.

First of all, we can calculate the current for each conductor of each turn. To do that, we must decide the number of series-turns N_s per pole. Looking at some constructor tables, we choose a round wire with a diameter $d_c = 1.4$ mm, the insulated wire's diameter measures $d_c^{iso} = 1.465$ mm. Choosing then a number of turns equal to $N_s = 117$, it results in an area of the copper of $A_{onlyCu} = 180.11$ mm^2; that with the insulation becomes $A_{Cu} = 197.22$ mm^2 (inside the limit of 200 mm^2). Finally, we can calculate the current at the rotor windings' terminals. Since this current is the current that will be the output current of the power converter to be designed, we call it I_{out}:

$$I_{out} = \frac{\text{A-turns per pole}}{N_s} = \frac{1900}{117} = 16.24 \text{ A}. \tag{3.1}$$

With a current density in the rotor's conductors, equal to:

$$J_r = \frac{\text{A-turns per pole}}{A_{onlyCu}} = \frac{1900}{180.11} = 10.55 \ \frac{\text{A}}{\text{mm}^2}. \tag{3.2}$$

Finally, only the output voltage is missing. For calculating this voltage, we have to compute the electric resistance of the rotor winding. We suppose the

rotor to be working at the temperature of 100°C. The copper's resistance at this temperature is equal to:

$$\begin{aligned}\rho_{Cu}^{100} &= \rho_{Cu}^{20} \cdot (1+\alpha(100-20)) = \\ &= 0.016(1+0.004(100-20)) = 0.02112 \ \frac{\Omega \cdot \text{mm}^2}{\text{m}}.\end{aligned} \tag{3.3}$$

Referring to fig. 3.2, and knowing that the machine is 90 mm long, the length of a turn's conductor can be approximated as follows:

$$l_{cond} = [(90+12)+(27+12)] \cdot 2 = 0.282 \text{ m}. \tag{3.4}$$

The resistance of a single pole is then:

$$R_{pole} = \rho_{Cu}^{100} \cdot N_s \frac{l_{cond}}{S_c} = 0.45267 \ \Omega, \tag{3.5}$$

with $S_c = 1.5394$ mm^2, area of a single copper wire. The resistance of the entire rotor finally results $R_r = 1.81068$ Ω, and the output voltage to have the required current I_{out}, is then equal to $V_{out} = 29.40$ V.

In summary, the converter that we are going to design must satisfy the requirements listed in table 3.1. The inputs V_{in} and I_{in}^{max} are the voltage range and the maximum current of the vehicle battery, respectively.

Requirement	Value
V_{in}	$42 \div 54$ V
I_{in}^{max}	360 A
V_{out}	29.40 V
I_{out}	16.24 A

Table 3.1

3.2. Full-Bridge Converter

The entire system is composed by a full-bridge dc-dc converter, which is fed by the main vehicle's battery and its function is to provide the excitation current to the rotor winding of the synchronous motor.

In the following tables are listed the known characteristics of the various components of this system.

Battery	
Voltage Range	$42 \div 54$ V
Max Current	360 A

Regarding the excitation winding of the motor, since it represents the load of the converter, the main values that we need to design the full-bridge are the output dc current I_{out} and the output dc voltage V_{out}. These values are found through the following electrical characteristics of the rotor pole.

	Value	**Units**
Total current per pole	1900	A
Number of turns per pole	117	-
Current per conductor	16.24	A
Current density (Max)	10	A/mm^2
Conductor's temperature	100	°C
Conductor's diameter	1.40	mm
Cu resistivity	0.02112	$\Omega mm^2/m$
Pole mean length	0.282	m
Excitation's voltage	29.4	V

Table 3.2

The dc-dc full-bridge converter [21] is represented in fig. 3.3. On the primary side, there is the so called full-bridge. It is composed by two legs; each leg has two switches. The left leg is composed by switch $T1$ and $T4$; the right leg by switch $T3$ and $T2$. Every switch has a free wheeling diode, so that the magnetic energy stored inside the transformer can flow back to the battery when all four switches are opened. On the secondary side, after the transformer, there is a Graetz Bridge rectifier, composed by two legs and four diodes. Finally, after the rectifier, there is an L-C filter. The input voltage is V_{in}. The output voltage and current are V_{out} and I_{out}, respectively. The transformer has N_1 turns on the primary side and N_2 turns on the secondary side; the turn's ratio is $n = N_1/N_2$.

The switches work with a frequency f. Switches $T1$ and $T2$ have the same turn on signal; as well as switches $T3$ and $T4$. Two switches of the same leg can not be closed at the same time; otherwise, the battery will be short circuited.

Referring to fig. 3.4, we can see how a full-bridge works.

The fundamental quantity for this converter is the *duty cycle D*. It represents how long a switch stays closed respect to the duration of its period. So

$$D = \frac{t_{on}}{T}. \tag{3.6}$$

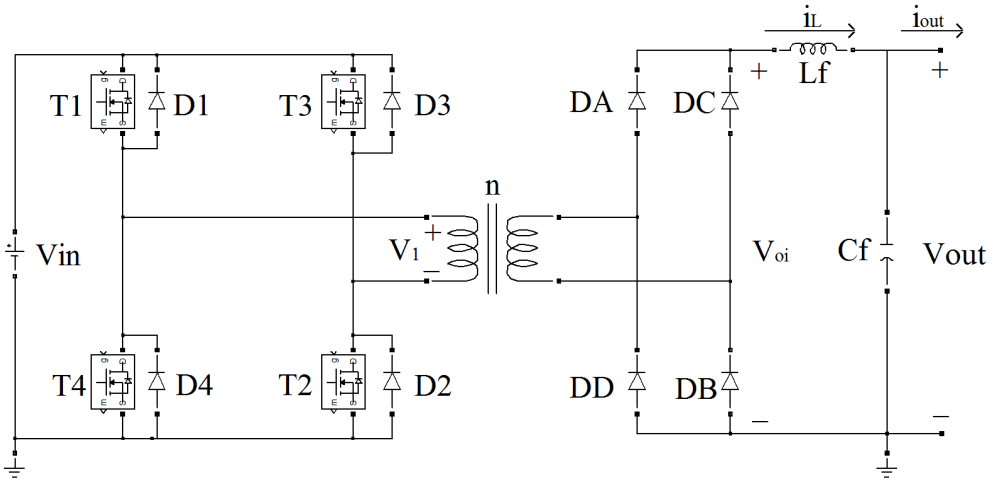

Figure 3.3: Dc-dc full-bridge schematic.

In this converter, every couple of switches, $T1$ and $T2$ or $T3$ and $T4$, stays open for up to half a semi-period, ideally. So, the duty cycle is always $D < 0.5$.

Looking at the first wave form in fig. 3.4, we can get to the fundamental relationship of the dc-dc full-bridge:

$$V_{out} = 2\frac{N_2}{N_1} \cdot D \cdot V_{in}. \tag{3.7}$$

From these relationships it is also possible to find the desired value of the choke inductance. From fig. 3.3 and fig. 3.4, the voltage across the inductance L_f is:

$$v_L(t) = v_{oi}(t) - v_{out}(t) = L_f \frac{di_L(t)}{dt}. \tag{3.8}$$

For a switch's pulse duration t_{on}, eq. (3.8) becomes:

$$\Delta i_L = \frac{1}{L_f}\left(\frac{N_2}{N_1}V_{in} - V_{out}\right) \cdot t_{on}. \tag{3.9}$$

But from eq. (3.6) and eq. (3.7):

$$t_{on} = \frac{N_1}{N_2}\frac{V_{out}}{V_{in}}\frac{1}{2f}. \tag{3.10}$$

Combining (3.9) and (3.10):

$$\Delta i_L = \frac{1}{L_f}\left(\frac{N_2}{N_1}V_{in} - V_{out}\right)\left(\frac{N_1}{N_2}\frac{V_{out}}{V_{in}}\frac{1}{2f}\right). \tag{3.11}$$

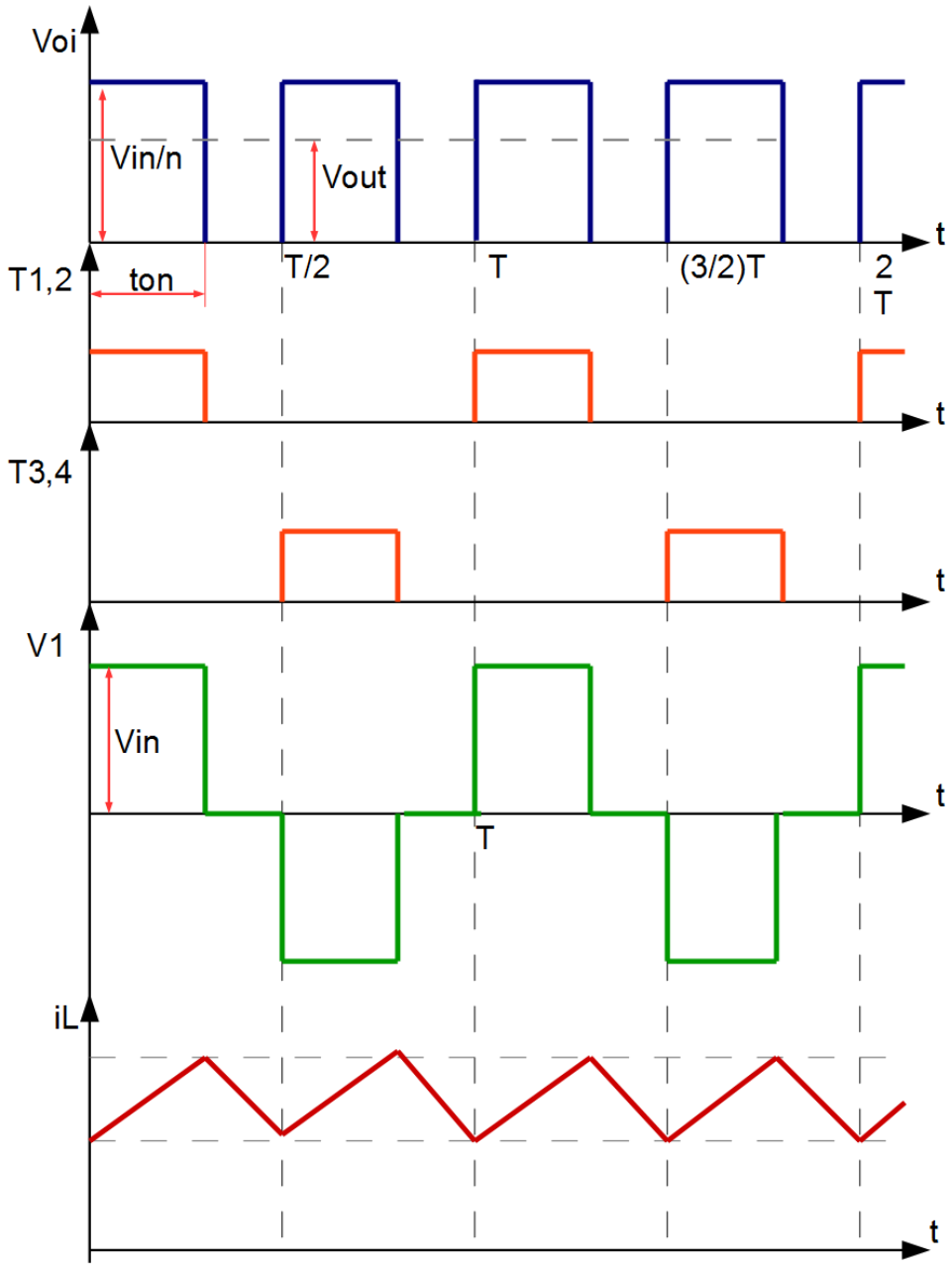

Figure 3.4: Dc-dc Full-bridge voltages and currents.

If I_{out} is known, we can put, for instance, $\Delta i_L = 0.2 \cdot I_{out}$, and find the corresponding value of L_f in order to obtain this deviation of the output current.

It is important to say that all these relationships are valid as long as the output

current is different from zero during all the period T. For light load working conditions, thus small duty cycles, it is possible that the current i_L falls to zero before the next couple of switches is switched on. This is called *discontinuous operation mode* and the equations above are no longer valid. Therefore, this occurrence is to be avoided (see [21]).

3.2.1. Frequency and magnetic core

In this work, and in general in automotive applications, it is important to limit the volumes and the weights. For this reason we will try to reduce the volume of the transformer. Since the cross sectional area of the transformer is inversely proportional to the frequency, the solution could be to use the highest frequency available. However, with the increase of frequency, they increase:

- the iron losses,
- the skin effect and thus the Joule losses,
- the eddy currents losses,
- the commutation losses on the switches.

Anyway, the hysteresis losses are also proportional to the volume of the iron core (see Appendix A).

If the request of a small volume is strong, it is important to reduce the losses in other ways, and to do an optimization in order to balance pros and cons of the high frequency. In our work, we can choose the range of frequencies that will be put inside the optimization, through the choice of the switches and of the material of the transformer's core.

The switches more suitable for medium voltages and medium power (around the kW) are the MOSFets: they have a medium-high range of frequencies, from the kHz to the MHz.

For medium-high frequency transformers, a very good option are *soft magnetic composites* such as the ferrites. We choose a ferrite called *T ferrite*® (Appendix A and [15]) because it has low hysteresis losses and negligible eddy currents.

Finally, comparing the features of the switches and of the ferrite, as well as the full-bridge converter, the range of frequencies suitable for this application is from the kHz to $30 \div 50$ kHz.

3.3. Soft switching: ZVT

With a rotary transformer or, in general, with a transformer with an air gap, there is a small main inductance that causes the flowing of high primary currents. This leads to elevated commutation and conduction losses in the full-bridge switches. In order to reduce the losses, and to avoid complex snubber circuitry, it is advised to implement a soft switching strategy. In fact, it is better to avoid the contemporary presence of current and voltage, when a switch commutates.

For this, we will exploit the parasitic elements of the circuit. In fact, with a small main inductance, in a rotary transformer, there is also a big leakage inductance. This inductance is in series with the primary side of the transformer, and, depending on the situation, it can be in series with another parasitic element in a full-bridge: the output capacitance C_{oss} of a MOSFet.

This capacitance is very useful because it is well known and it does not change much during the converter's operation. The leakage inductance varies with the geometry of the transformer.

The strategy that can be used here is called *Zero Voltage Transition*, ZVT [13] [8]. It is a fixed frequency strategy, that allows to switch on a MOSFet with a zero voltage across it, using the resonant transition between the output capacitance and the leakage inductance. For that, it works only for a certain range of frequencies.

The ZVT fundamentals are the following. Rather than driving the diagonal switches together, there is a phase delay that makes, for a short period of time, the primary side short circuited. In this time there is the resonant transition that puts all the switches of the other diagonal switches at zero voltage before they turn on.

We make an example, referring to figure 3.3 and figure 3.5. V_a is the voltage at the upper terminal of the primary side of the transformer, V_b at the lower terminal.

- before the time t_0 there is the power transfer interval. $T1$ and $T2$ are still closed and the current on the primary side is $I_P(t_0)$.

- $t_0 < t < t_1$, *resonant transition interval*, $T2$ =off=open, $T1$ =on=closed. The current is kept almost constant by the leakage inductance and it flows through the output capacitance of switches 2 and 3. In this way the voltage across $T2$ goes to V_{in} and the voltage across $T3$ falls to zero, allowing a zero voltage switching. During this interval also the voltage across the primary side will fall to zero.

- $t_1 < t < t_2$, *clamped free wheeling interval*, $T1$ =on, $T3$ =on, $D3$ =on. $T3$ is switched loss-less for the zero voltage across it. The current is again almost constant and it is split between $T3$ and $D3$. This interval is needed to keep the frequency constant.

- before the new power transfer, the same is done for switches $T3$ and $T4$ in order to close loss-less the switch $T4$.

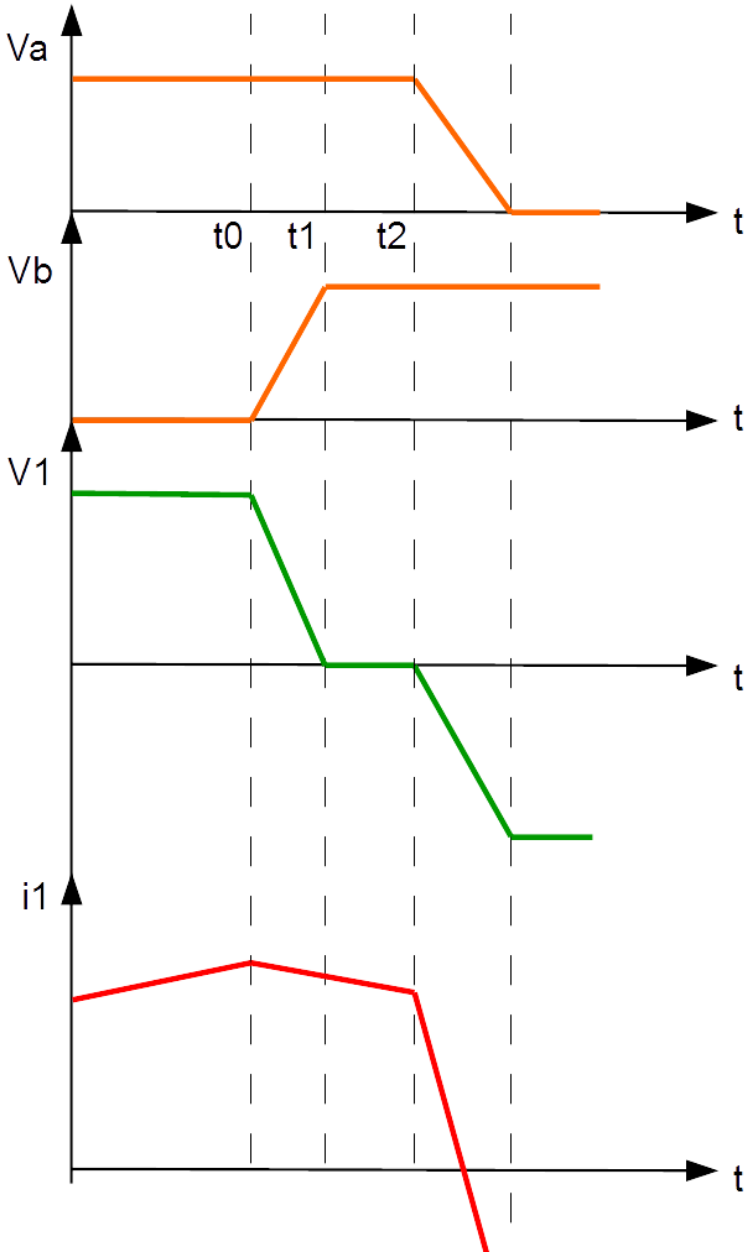

Figure 3.5: A transition interval for the ZVT.

3.3.1. ZVT requirements

In order to achieve the ZVT, the energy stored inside the leakage inductance L_{lk} must be more than the energy stored inside the equivalent series capacitance C_R.

The resonant tank frequency is:

$$\omega_R = \frac{1}{\sqrt{L_{lk} \cdot C_R}}. \tag{3.12}$$

We call t_{max}, the maximum time needed for each resonant transition, which must be [13]:

$$t_{max} = \frac{\pi}{2\omega_R}. \tag{3.13}$$

If we assume a maximum value for the duty cycle, occurring for light loads, t_{max} can be estimated as follows [8]:

$$D_{max} = \frac{1}{2} - \frac{t_{max}}{T}. \tag{3.14}$$

The resonant capacitance is then:

$$C_R \simeq \frac{8}{3} \cdot C_{oss}. \tag{3.15}$$

Finally, combining the previous expressions, the minimum value required for the leakage inductance in order to accomplish the resonant transition is:

$$L_{req} \simeq \frac{1}{\left(\frac{\pi}{2 \cdot t_{max}}\right)^2 \cdot \frac{8}{3} \cdot C_{oss}}. \tag{3.16}$$

During the design, with the help of the optimization, we will try to build a geometry that gives a leakage inductance similar to L_{req}. In this way it could be possible to use favorably a parasitic element such as the leakage inductance, to achieve soft switching without the necessity to add an external inductance.

CHAPTER 4

Rotary Transformer Design

The rotary transformers are already used in some specific applications, such as video recorders or spatial machinery with rotating parts. Only in the last years, there were some publications about using them as excitation means for electrical rotating machines. Because of this marginal utilization, there is not much literature about how to best design them.

Anyway, it is normally possible to design a rotary transformer in the same way as a traditional transformer with an air gap. For instance, for the pot core it is possible to use the already existing commercial pot cores, adding afterward the air gap [23].

In this particular case though, we will proceed with an optimization , followed by a finite element analysis. The main reasons for such a procedure are: the need of an optimized volume for the *ELANi Machine* size issues, and the possibility to implement the ZVT in the converter.

4.1. Analytical Models

In this section, we will see how a rotary transformer can be synthesized and treated analytically. We will compute the inductances (leakage and main), the resistive losses, and the iron losses of the ferrite core. This is useful in this work for two reasons. First, we can use the analytical calculated characteristics to have an idea of the best way to proceed in the design; for instance, estimating the losses we can forecast the efficiency and choose a proper material for the magnetic core. Secondly, we can use analytical expressions of some quantities in the optimization,

or, if there is no need of an optimized design, in the design process. For example, the efficiency could be used as a fitness function in the optimization.

In the following pages, all the symbols used to describe the geometry of the two typologies of transformers, are depicted in figures 4.1 and 4.2.

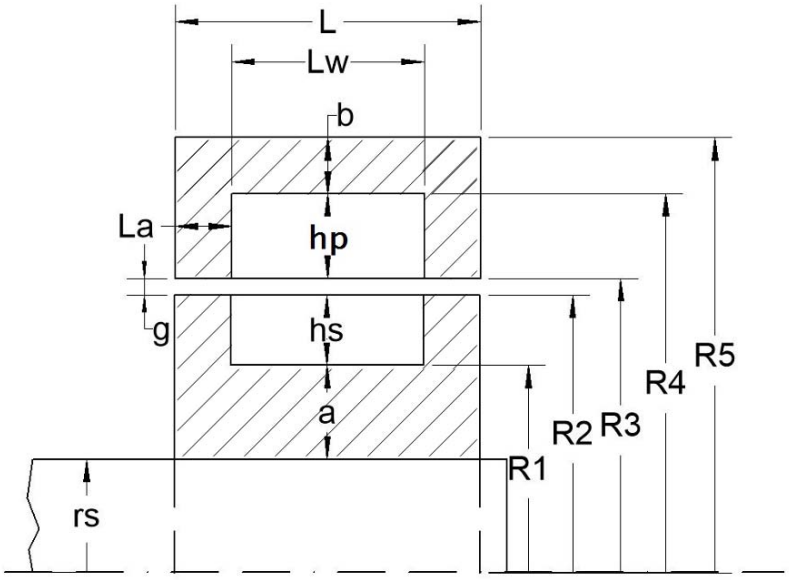

Figure 4.1: Side view of an axial rotating transformer.

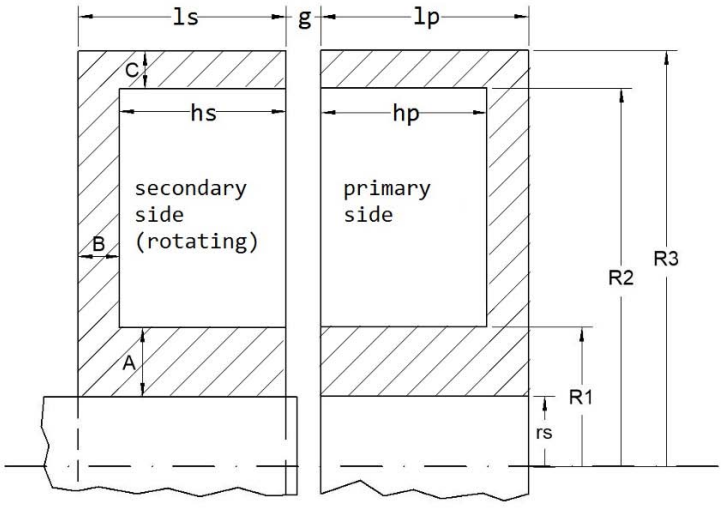

Figure 4.2: Side view of a pot core rotating transformer.

4.1.1. Equivalent circuit

Every transformer can be ideally considered as a two-port inductive component [4]. In this case, it is a single-phase transformer with an air gap. Neglecting the iron losses and the saturation effects of the ferrite, the transformer has the equivalent circuit shown in fig. 4.3.

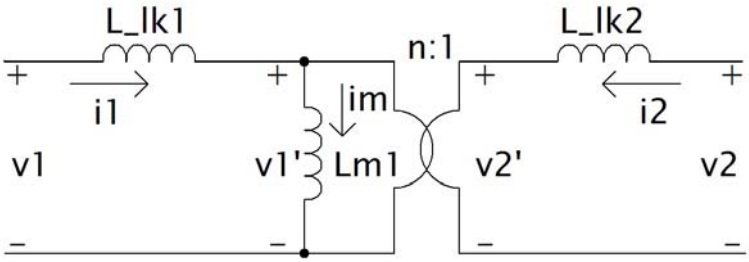

Figure 4.3: Equivalent T circuit of the transformer as a two-port inductive component.

At the two-port component terminals we have the following voltages.

$$\begin{cases} v_1 = \frac{d\lambda_1}{dt} = L_1 \frac{di_1}{dt} + M \frac{di_2}{dt} \\ v_2 = \frac{d\lambda_2}{dt} = M \frac{di_1}{dt} + L_2 \frac{di_2}{dt} \end{cases} \tag{4.1}$$

With L_1 and L_2 self-inductances of the primary and of the secondary side respectively, M mutual-inductance, and, λ_1 and λ_2, linked fluxes. This fluxes can also be expressed like in equation (4.2).

$$\begin{cases} \lambda_1 = L_1 i_1 + M i_2 \\ \lambda_2 = M i_1 + L_2 i_2 \end{cases} \tag{4.2}$$

The two self-inductances can be arbitrarily split up in two factors. One, L_{lkx}, represents the leakage inductance, referred to the lost magnetic flux. The other factor L_{mx}, represents the magnetizing (or main) inductance, thus related to the energy needed to magnetize the core of the transformer.

Usually, in order to represent an ideal transformer, the subdivision is the following

$$\begin{cases} L_1 = L_{lk1} + L_{m1} \\ L_2 = L_{lk2} + L_{m2} \end{cases} \tag{4.3}$$

with always

$$L_{m1} \cdot L_{m2} = M^2.$$

This is an ideal representation of the transformer, that assumes the presence of a primary leakage inductance L_{lk1} and a primary main inductance L_{m1}, and a secondary leakage inductance L_{lk2} and a secondary main inductance L_{m2}. With this hypothesis, the transformer can be represented like in fig. 4.3, where $n = \frac{L_{m1}}{M} = \frac{M}{L_{m2}}$ is the ideal transformation ratio, and

$$\begin{cases} v_1' = n \cdot v_2' \\ i_m = i_1 + \frac{i_2}{n}. \end{cases} \tag{4.4}$$

The subdivision in equation (4.3), in leakage and main inductances is arbitrary, as long as equation (4.2) is true, and the inductances' values are positive, or at least equal to zero.

A common choice is to set $n = \frac{N_1}{N_2}$, and to refer all the quantities of the equivalent circuit to the primary side. To do that we impose

$$n' = \frac{M}{L_2}$$

so that the secondary leakage inductance is equal to zero and we can use the equivalent circuit in fig. 4.4.

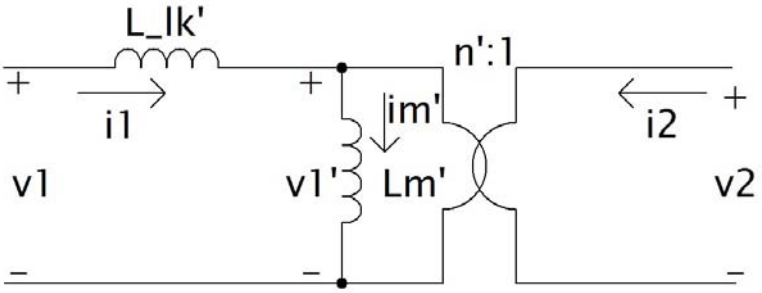

Figure 4.4: Equivalent Γ circuit of the transformer.

With the finite element analysis, we will simulate the transformer with first the secondary side, and then the primary side open, in order to find the self and mutual inductances of the two-port inductive component: L_1, L_2, and M. Then we will use the following equalities to *"take"* them in the Γ equivalent circuit of fig. 4.4.

$$L_m' = \frac{M^2}{L_2}, \qquad L_{lk}' = \frac{L_1 \cdot L_2 - M^2}{L_2}. \tag{4.5}$$

In the analytical discussion, we will find directly the Γ inductances, L_{lk}' and L_m', and we will call them L_{lk} and L_m.

4.1.2. Leakage inductances

The analytical computation of the leakage inductances is inaccurate because the leakage flux lines paths are not well known, at least before the finite element analysis. Actually, also the values of the inductances of a transformer calculated through the FEA are often different from the values found on the real machine.

The calculation of the leakage inductance is done here for a pot core; for the axial type the procedure is similar, so that we explain exhaustively only the first one, and write only the final expression for the second one.

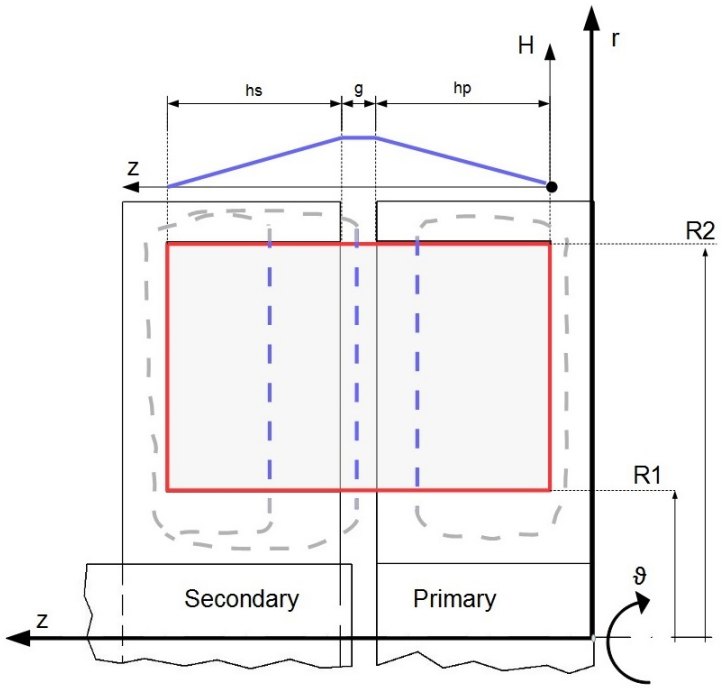

Figure 4.5: Flux lines taken into account for the pot core transformer's leakage inductance.

Referring to fig. 4.5, the leakage inductances are calculated through the magnetic energy stored inside the volume of the windings and of the air gap (delimited by the red borderline), that is supposed to be the same energy stored by the leakage inductances [5] [3]. The side effects are not taken into account.

$$W_m = \int_v \frac{1}{2}\mathbf{H}\cdot\mathbf{B}\,\mathrm{d}v = \frac{1}{2}L_{lk}I^2. \tag{4.6}$$

In the air gap, see fig. 4.5, the magnetic field H is supposed constant, and

equal to[1]:

$$H_g = \frac{N_1 \cdot I_1}{g}. \tag{4.7}$$

In the windings the field varies linearly with the axial length of the coils, $R2 - R1$. For the primary side is:

$$H_p = \frac{N_1 \cdot I_1}{R2 - R1} \cdot \frac{z}{h_p}. \tag{4.8}$$

And for the secondary side:

$$H_s = \frac{N_1 \cdot I_1}{R2 - R1} \cdot \frac{z}{h_s}. \tag{4.9}$$

In average, equation (4.6) can be written as:

$$W_m = \frac{1}{2}\mu_0 H^2 \cdot Vol = \frac{1}{2} L_{lk} I^2. \tag{4.10}$$

So, the average of the flux in the primary coil is:

$$\langle H_p^2 \rangle = \frac{N1^2 \cdot I_1^2}{(R2 - R1)^2} \cdot \frac{1}{h_p} \int_0^{h_p} \frac{z^2}{h_p^2} \, \mathrm{d}z = \frac{N1^2 \cdot I_1^2}{(R2 - R1)^2} \cdot \frac{1}{3}. \tag{4.11}$$

The same expression can be found for the secondary coil.

If we put the three values of H^2 in equation (4.10), we obtain:

$$W_m = \frac{1}{2}\mu_0 \frac{N1^2 \cdot I_1^2}{(R2 - R1)^2} \left[\frac{h_p}{3} MLT + \frac{h_s}{3} MLT + g \cdot MLT \right]. \tag{4.12}$$

With MLT =mean length turn of the volume (coils and air gap).

Referring to fig. 4.2 and fig. 4.1, the expressions of the leakage inductances are therefore the following.

For the Pot Core transformer:

$$L_{lk} = \mu_0 N_1^2 \cdot \frac{MLT}{R2 - R1} \left(g + \frac{h_s + h_p}{3} \right) \cdot 10^{-3} \text{ in [H]}, \tag{4.13}$$

[1] We use Ampere's Law:

$$\oint_{\partial S} \mathbf{H} \cdot \mathrm{d}\mathbf{l} = NI,$$

but we consider only the field inside the coils volume, and the permeability of the ferrite core is supposed so high as to be able to neglect the magnetic voltage drop in the ferromagnetic material. Therefore:

$$H = \frac{NI}{l}$$

.

with all the dimensions in $[mm]$ and $MLT = \pi(R2+R1)$.

For the Axial transformer:

$$L_{lk} = \mu_0 N_1^2 \cdot \frac{MLT}{L_w} \left(g + \frac{h_s + h_p}{3} \right) \cdot 10^{-3}, \tag{4.14}$$

with $MLT = \pi(R4+R1)$.

4.1.3. Magnetizing inductances

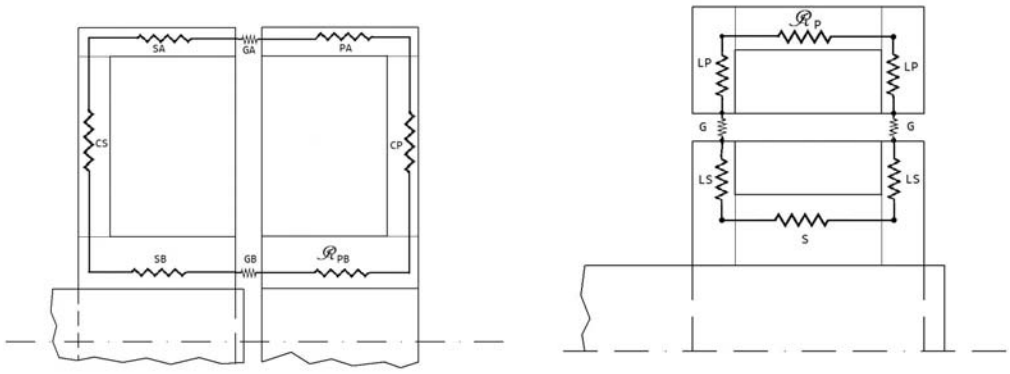

(a) Pot Core. (b) Axial.

Figure 4.6: Reluctance network for both transformers.

The magnetizing inductances are computed through the equivalent magnetic circuit of the transformer's core. Therefore, we compute all the values of reluctance of each section of the core as follows:

$$\mathscr{R} = \int_{\partial S} \frac{dl}{\mu \cdot S}. \tag{4.15}$$

The equivalent reluctance network for each transformer can be seen in fig. 4.6. For the calculation of each reluctance, the dl that we use for every part of the magnetic core is the length of the reluctance symbol in the pictures.

Pot Core Main Inductance Referring to fig. 4.6*a*:

$$L_m = \frac{N_1^2}{\mathscr{R}_{CS} + \mathscr{R}_{CP} + \mathscr{R}_{SB} + \mathscr{R}_{PB} + \mathscr{R}_{SA} + \mathscr{R}_{PA} + \mathscr{R}_{GA} + \mathscr{R}_{GB}}, \tag{4.16}$$

with,

$$\mathscr{R}_{CS} = \frac{R2 - R1}{2\pi\mu(l_s - h_s)} \cdot \ln\frac{R2}{R1},$$
$$\mathscr{R}_{CP} = \frac{R2 - R1}{2\pi\mu(l_p - h_p)} \cdot \ln\frac{R2}{R1},$$

$$\mathscr{R}_{SB} = \frac{l_s}{\mu\pi(R1^2 - r_s^2)}, \quad \mathscr{R}_{PB} = \frac{l_p}{\mu\pi(R1^2 - r_s^2)}, \quad \mathscr{R}_{SA} = \frac{l_s}{\mu\pi(R3^2 - R2^2)},$$
$$\mathscr{R}_{PA} = \frac{l_p}{\mu\pi(R3^2 - R2^2)}, \quad \mathscr{R}_{GA} = \frac{g}{\mu_0\pi(R3^2 - R2^2)}, \quad \mathscr{R}_{GB} = \frac{g}{\mu_0\pi(R1^2 - r_s^2)}.$$

Axial Main Inductance Referring to fig. 4.6*b* :

$$L_m = \frac{N_1^2}{\mathscr{R}_S + \mathscr{R}_P + 2\mathscr{R}_G + 2\mathscr{R}_{LS} + 2\mathscr{R}_{LP}}, \tag{4.17}$$

with,

$$\mathscr{R}_S = \frac{L_w}{\mu\pi(R1^2 - r_s^2)}, \qquad \mathscr{R}_P = \frac{L_w}{\mu\pi(R5^2 - R4^2)},$$

$$\mathscr{R}_{LS} = \frac{R2 - r_s}{\mu 2\pi L_a} \cdot \ln\frac{R2}{r_s}, \quad \mathscr{R}_{LP} = \frac{R5 - R3}{\mu 2\pi L_a} \cdot \ln\frac{R5}{R3}, \quad \mathscr{R}_G = \frac{g}{\mu_0 2\pi L_a} \cdot \ln\frac{R3}{R2}.$$

4.2. Optimization

In order to find an initial, but proper, geometry for the transformer, we choose to do an optimization. This procedure is preferred in this case because we want to fulfill various objectives at the same time. In fact, we want to:

- respect size limits;
- try to build a geometry that allows to have enough leakage inductance on the primary side, in order to reach the soft switching requirements.

Beside that, it is difficult to find literature about rotary transformers and how to design them.

In general, the optimization wants to minimize one or more functions, called *objective functions* or, in our case, *fitness functions*. The value of these functions depends on many parameters, or a *set* of parameters: the final goal is to find the values of these parameters that make the fitness function minimal.

There are many approaches for the optimization. In this work we consider:

- a *single objective optimization*, with a single fitness function and hence a unique solution;
- a *weighted approach*, which uses a single objective optimization, but the fitness function is a sum of weighted multiple objective functions;
- a *multi-objective optimization*, with multiple fitness functions and many results.

In the following pages, we refer to MATLAB®'s Toolboxes for the optimization [16]. For all three approaches, it is used the same optimization algorithm: the *genetic algorithm*.

4.2.1. Genetic algorithm

The main unit for the genetic algorithm is the *individual*. It is a set (vector) of variables to which you can apply the fitness function. Each individual has a *score*, which is the value of the fitness function evaluated at the individual's point.

An array of individuals is called *population*. At each iteration, the genetic algorithm evaluate a series of characteristics of the individuals in order to properly generate a new population, called *new generation*.

In order to create the new generation, the algorithm chooses from the group of individuals the so called *parents*, and uses them to create new individuals, called *children*.

Since the algorithm wants to find the fitness function's minimum, the best parents are the individuals with a low score, or *fitness value*. The individuals with the lowest fitness values are called *elite* and they are passed directly to the next population.

Children are produced by:

- *mutation*: random changes to a single parent;
- *crossover*: combining a pair of parents. Takes randomly into the new child's vector, the coordinates of the two parents' vector.

The optimization stops when it reaches the *stopping conditions*:

- max number of generations;
- time limit;
- fitness limit: if the score of the individuals reaches the minimum value of the objective function (usually set to -Inf);
- stall generations: the average weighted change in subsequent generations falls below a limit.

Usually, it is possible to modify all these values; in this work the default values are set.

4.2.2. Single objective genetic algorithm

In this work it is used the single objective optimization, with the genetic algorithm. The other two possibilities, the multiobjective optimization and the weighted approach, are not used. Their description and the explanation of why they are not used, are in Appendix B.

The crucial point of an optimization is the *fitness function*. For this work, we use the *volume* of the transformer as objective function.

Since the ELANi machine has size issues, it could be more appropriate to choose the length of the transformer as fitness function. But we want to be here as much general as possible. Beside that, it is unknown the exact volume reserved for the converter, nor the dimensions of the end windings of the motor. In fact, two possible configurations of the rotary transformer inside the machine, are depicted in fig. 4.7. It could be possible to put a transformer with a small diameter inside the end windings of the rotor, or to put a rotary transformer with high diameter and small length in the same position of the slip rings system. But since we do not know the precise geometry of the whole system, we will minimize the volume.

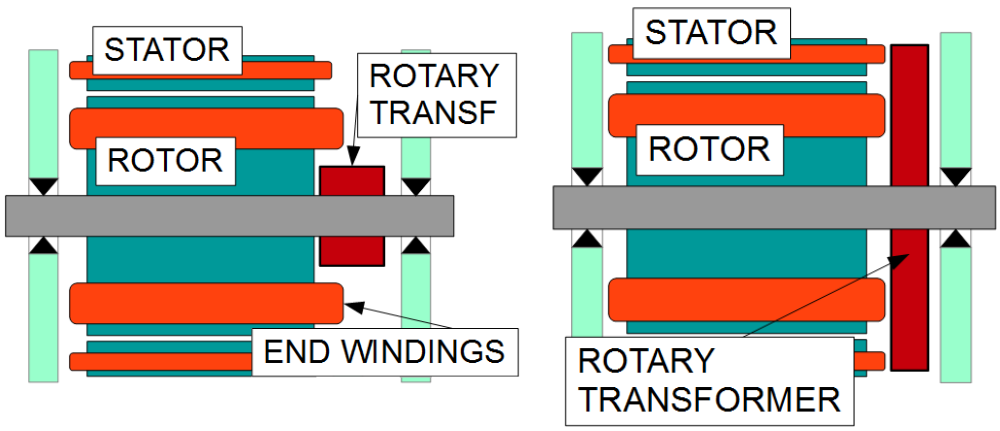

(a) (b)

Figure 4.7: The rotary transformer inside the machine.

The single objective optimization algorithm, called *ga*, has the following inputs:

1. the fitness function $f(\bar{x})$, dependent on the variables for which we want to find the optimal values;
2. the number of variables $\bar{x} = x_1, x_2, x_3, \ldots$;
3. linear inequalities, represented as a matrix inequality $[A]\{x\} \leq \{b\}$;
4. linear equalities, $[A]\{x\} = \{b\}$;
5. non-linear constraints functions, $ceq(\bar{x}) = 0$;
6. upper *ub*, and lower *lb*, bounds for the variables' vector.

There are some considerations that are made before the optimization, in order to set the correct values for the algorithm's inputs.

The starting point of the design of a transformer is the choice of the cross sectional area, around which are wound the conductors, that is needed to convey the magnetic flux in order to have enough power transfer without saturating the magnetic material. The section of ferrite needed, can be found easily thanks to the fact that we are using a full-bridge converter, with a quasi-square wave voltage at the transformer's terminals [24] [17].

We start with Faraday's law, and, on average, for a time step Δt, the back e.m.f. E results:

$$E\Delta t = -N \cdot A_c \cdot \Delta B, \ [\mathrm{Vs}]\,. \tag{4.18}$$

Usually then, the back e.m.f. is equal and opposite to the applied voltage V_{in} and, for a square wave, the pulse duration is $t_{on} = \Delta t$:

$$\Delta B = \frac{V_{in} \cdot t_{on}}{N \cdot A_c}, \ [\mathrm{T}]. \tag{4.19}$$

Now, ΔB is here the peak-to-peak value of the entire B-H characteristic; so $\Delta B = 2 \cdot B_{sat}$, where B_{sat} is the saturation flux density of the ferrite. Furthermore, for a full-bridge, the pulse duration is a function of the duty cycle and of the frequency: $D = t_{on} \cdot f$. Rearranging the previous equations, we have:

$$A_c = \frac{V_{in} \cdot D}{2 \cdot N_1 \cdot f \cdot B_{sat}}, \ \left[\mathrm{m}^2\right]. \tag{4.20}$$

There are some assumptions that are the same for both kinds of transformer. First of all, the transformer's number of turns, or the turn ratio, $n = \frac{N_1}{N_2}$. For a full-bridge, the fundamental equation is:

$$V_{out} = 2\frac{N_2}{N_1} \cdot D \cdot V_{in}. \tag{4.21}$$

With D, the duty cycle, V_{in}, the battery's voltage, and V_{out}, representing the excitation voltage. Supposing a maximum duty cycle of 0.43, corresponding to the minimum battery voltage, the ratio must be:

$$n \leq 2 \cdot D_{max} \frac{V_{in}}{V_{out}} \leq 1.23. \tag{4.22}$$

We choose a value of 1.2 for n, and therefore a value of 6 and 5 for N_1 and N_2, respectively. Bigger values are not allowed because of the limit on the volume and because, if N_1 is bigger, the area of the ferrite core will result too thin also for relatively low frequencies (see eq. 4.20).

Other assumptions for both transformers are:

- the value of the maximum flux density, in order not to saturate the core, is 0.25 T (the saturation value is 530 mT, but it is customary to use in the design phase less than half the saturation flux density);
- the same conductor's diameter for both primary and secondary side, $d =$ 1.60 mm;
- the fill factor k_f for the transformer's slots equal to 0.45;
- the radius of the shaft $r_s = 9$ mm;
- the air gap length $g = 0.6$ mm;

- maximum axial length of the transformer of 23 mm;
- maximum diameter of the transformer of 90 mm.

It is important to point up that these assumptions, in particular the flux density and the diameter of the wires, are needed only for the optimization purposes. During the later design, they may change.

4.2.3. Pot core transformer optimization

Variables

For the Pot Core there are 7 variables, so that the results vector of the optimization will be:

$x(1)$	$x(2)$	$x(3)$	$x(4)$	$x(5)$	$x(6)$	$x(7)$
$R1$	$R2$	$R3$	h_p	h_s	l_p	l_s

Fitness function

The volume's function has to be minimized:

$$volume(\boldsymbol{x}) = \pi \cdot R3^2(l_s + l_p + g). \tag{4.23}$$

Inequalities

$[A]\{x\} \leq \{b\}$
The inequalities that we set are all geometrical. The maximum length of the transformer can be 23 mm and the maximum diameter is 90 mm, therefore the maximum radius $R3$ is 45 mm.

$$\begin{cases} R3 \leq 45 \text{ mm} \\ l_s + l_p + g \leq 23 \text{ mm} \\ R1 < R2 < R3 \\ h_s < l_s \\ h_p < l_p \end{cases}$$

The relationship $[A]\{x\} \leq \{b\}$ is the following:

$$\begin{bmatrix} 0 & 0 & 1 & 0 & 0 & 0 & 0 \\ 0 & 0 & 0 & 0 & 0 & 1 & 1 \\ 1 & -1 & 0 & 0 & 0 & 0 & 0 \\ 0 & -1 & 1 & 0 & 0 & 0 & 0 \\ 0 & 0 & 0 & 0 & -1 & 0 & 1 \\ 0 & 0 & 0 & -1 & 0 & 1 & 0 \end{bmatrix} \{\mathbf{x}\} \leq \begin{bmatrix} 45 \\ 22.4 \\ 0 \\ 0 \\ 0 \\ 0 \end{bmatrix}$$

Equalities

$[A]\{x\} = \{b\}$

1. Since the quantity $R2 - R1$ and the cross section of the conductors are the same for both primary side and secondary side, and the transformer turn ratio is $n = 1.2$, it is possible to set the equality $h_p = 1.2 \cdot h_s$.

2. From the computed cross sectional area of the core A_c, it can be obtained the value of $R1$:
$$A_c = \pi(R1^2 - r_s^2).$$
So, $x(1) = R1$.

3. For commercial pot core transformers there are common relationships between different sections of the core. Typical values are used:
$$\begin{cases} B = 0.75A; \\ C = 0.60A. \end{cases}$$
If $A = R1 - r_s$, in the equalities matrix, there are the following:
$$\begin{cases} R3 - R2 = B; \\ l_p - h_p = C; \\ l_s - h_s = C. \end{cases}$$

Gathering this equalities, it results a matrix similar to the one above.

Lower bounds

In order not to compute negative solutions, all the lower bounds are set to zero. All except for h_p and h_s, for which are set higher limits in order to have the space to place at least two and one layers of conductors in the transformer's slots, respectively.

Upper bounds

Since the objective of the optimization is to minimize the volume, the upper bounds are not necessary.

Non-linear constraints

The non-linear constraints are called through a function and they are written in the form $ceq(\bar{x}) = 0$. We must now set three functions; the first two concern the relationship between the required area of the copper and the geometrical section of the slot:

1. $$(R2 - R1) \cdot h_p = \frac{N_1 \cdot A_w}{k_f};$$

2. $$(R2 - R1) \cdot h_s = \frac{N_2 \cdot A_w}{k_f}.$$

3. With the aim to get the required value of leakage inductance needed to make the ZVT work, the expression of the leakage inductance, function of the geometry of the windings, is set equal to the value computed analytically, function of the frequency and of the MOSFet output capacitance, C_{oss}.
   With reference to the fig. 4.2:

   $$L_{lk} = \mu_0 \cdot N_1^2 \cdot \frac{MLT}{R2 - R1} \cdot \left(g + \frac{h_p + h_s}{3} \right) \cdot 10^{-3} = L_{req}(f, C_{oss}),$$

   with $MLT =$ mean length turn of the windings$= \pi(R2 + R1)$. All the sizes are in mm and the result is in Henry.

4.2.4. Axial transformer optimization

Variables

For the Axial transformer there are 6 variables, so that the results vector will be:

$x(1)$	$x(2)$	$x(3)$	$x(4)$	$x(5)$	$x(6)$
a	h_s	h_p	b	L_w	L_a

Fitness function

The volume's function has to be minimized:

$$volume(\boldsymbol{x}) = \pi(r_s + a + h_s + g + h_p + b) \cdot (2L_a + L_w). \tag{4.24}$$

Inequalities

$[A]\{x\} \leq \{b\}$

The only inequalities that we must set for this optimization, are due to the limits on length and diameter. So:

$$\begin{cases} r_s + a + h_s + g + h_p + b \leq 45 \text{ mm} \\ 2L_a + L_w \leq 23 \text{ mm}. \end{cases}$$

For the optimization, we can build a matrix similar to the matrix of the pot core.

Equalities

$[A]\{x\} = \{b\}$
As for the pot core, the value $R1$, and consequently the variable $a = R1 - r_s$, can be found through the cross sectional area of the core. Another similar equality is the one regarding the area of the slots.

Finally, even for this kind of transformer, we set typical commercial pot core relationships between the different parts of the ferrite core. In particular, L_a and b are 0.6 times the computed value of a.

Lower and upper bounds

We can find the optimization boundaries for the axial transformer in the same way of the pot core's ones. So they are:

$$lb = [0, 1.8, 3.4, 0, 3.4, 0];$$

$$ub = [\,].$$

Non-linear constraints

Also for the axial transformer, there are three non-linear constraints. The first two, as for the pot core, are about the minimum area of copper, given the number of turns. The third one is the expression of the leakage inductance:

$$L_{lk} = \mu_0 \cdot N_1^2 \cdot \frac{\pi(2r_s + 2a + h_s + h_p + g)}{L_w} \cdot \left(g + \frac{h_p + h_s}{3}\right) \cdot 10^{-3} = L_{req}(f, C_{oss}).$$

All the sizes are in mm and the result is in Henry.

4.2.5. Optimization's script

After having set the optimization inputs, we want to find the best geometry for the transformer. Looking at equation (4.20), we see that the only value that is not decided is the working frequency of the transformer.

In order to see all the possible solutions and geometrical configuration of the transformer, we put the optimization algorithm inside a for cycle of frequencies. For each frequency is first computed the cross sectional area of the core. The result of this calculation complete the inputs for the optimization algorithm. The *ga* optimization finally finds an optimal geometry for the transformer.

Given the geometrical characteristics of a transformer, for every frequency:

- the leakage inductances with the expressions in section 4.1.2,
- the main inductances as described in section 4.1.3,
- an approximated evaluation of the Joule losses,
- the iron losses,

are computed.

The resistive losses (Joule losses) are computed as follows:

$$P_J = \rho \cdot \pi D_m \cdot A_{Cu} \cdot J^2, \tag{4.25}$$

with $\rho = 0.02112\ \Omega\text{mm}^2/\text{m}$, $D_m =$ mean diameter of the coils in meters, A_{Cu} area of the copper and J current density. It is important to say that in the first optimization we do not know in advance the exact value of the currents in the transformer's coils; so we put here a constant current density of $10\ \text{A}/\text{mm}^2$, equal to the maximum value allowed.

The iron losses are computed through the Steinmetz simplified expression, typical for the chosen ferrite (see Appendix A):

$$P_{iron} = C(T) \cdot f^{\alpha} \cdot B^{\beta} \cdot Volume. \tag{4.26}$$

where $C(T)$ is a temperature depending constant, at 100°C equal to $3.354\ \text{mW}/\text{cm}^3$, α is equal to 1.926 for f in kHz and β to 2.731 for B in Tesla.

4.2.6. Optimization's Results

With the optimization, we want to find the frequency that leads to the best geometry. So the first result to stress, is the range of frequencies taken into account by the optimization script.

For both transformers, the lower limit of frequency is set by the maximum size of the transformer. Below a certain frequency, one size limit, length or diameter, is not respected.

The upper limit, in general, can be set accordingly to the maximum switching frequency of the converter's switches, or to mechanical limitations. In fact, with higher values of frequency, we have smaller cross sectional area of the ferrite core, and so smaller thickness of the ferrite. Looking at constructor's data-sheets of ferrite transformers, we set the minimum thickness of the ferrite at 2.5 mm. Furthermore, an easy and approximated mechanical calculation has been done to check the resistance of such a thickness of the ferrite under rotational stresses (see Appendix A).

The range of frequencies simulated is then the following.

	Lower Limit	Upper Limit
Pot Core	7000 Hz	30000 Hz
Axial	4000 Hz	30000 Hz

Choosing the optimal frequency

Since we have chosen a single objective optimization, in order to find the best transformer amongst the ones with the optimal volumes, and thus the best frequency, we can add another fitness function outside the optimization: the efficiency.

Hence, we can plot the losses, resistive and iron losses, for each frequency. The optimal transformer will be the one with the lower losses. In fig. 4.8, we can see that, for the pot core, the optimal frequency is around 55 kHz. The same result is achieved for the axial transformer. The Joule losses decrease with the frequency, because the mean diameter of the windings decreases with the frequency. Conversely, the iron losses are proportional to the power of the frequency, and then they grow.

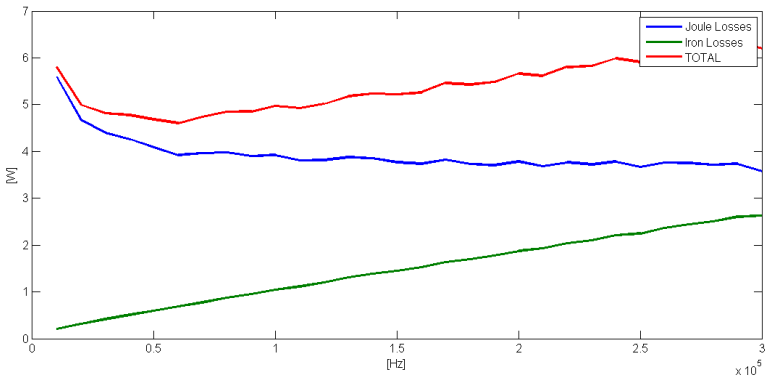

Figure 4.8: Analytical losses for the optimal pot core, for each frequency.

However, this frequency leads to a minimum thickness of the ferrite core, lower than 2.5 mm. So, the criterion becomes the minimum core thickness of 2.5 mm, at the maximum frequency allowable with this limit, because below 55 kHz the losses decrease with the frequency.

This limit is reached for both transformers at 20.5 kHz. The optimal transformers with the minimum volume for 20.5 kHz are depicted in fig. 4.9.

In table 4.1 are listed the analytical calculations of some important values for both transformers. Regarding the losses, the pot core seems to be more efficient than the axial. But it is axially longer and, in general, it has a bigger volume for the same frequency.

However, the most important value in table 4.1 is the leakage inductance. In fact, we see that the required value for the ZVT is in general very high, and, in particular, it is much higher than the transformer's leakage inductance. Therefore, in order to achieve the ZVT, it is necessary an external inductance.

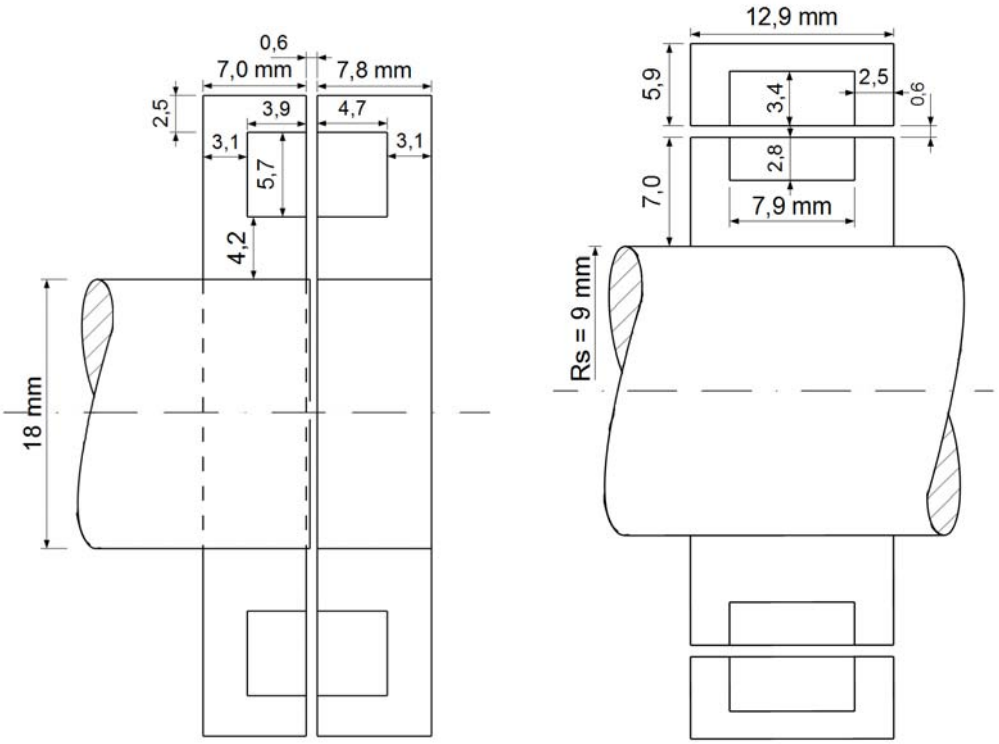

(a) Optimal pot core.

(b) Optimal axial.

Figure 4.9: Optimal transformers from the analytical optimization.

	Pot Core	Axial
Joule Losses	4.7080 W	4.8700 W
Iron Losses	0.3224 W	0.2887 W
Axial length	15.4 mm	12.9 mm
Maximum radius	21.4 mm	22.5 mm
Volume	22156 mm^2	20516 mm^2
Leakage induct. ZVT	0.2597 H	0.2597 H
Leakage induct. computed	$4.88 \cdot 10^{-7}$ H	$1.60 \cdot 10^{-6}$ H

Table 4.1

It is possible now to do some preliminary comparisons between the pot core typology and the axial one. For instance in fig. 4.10, 4.11, and 4.12, we can see how the different kind of losses evolve with the computed frequencies, for the two transformers.

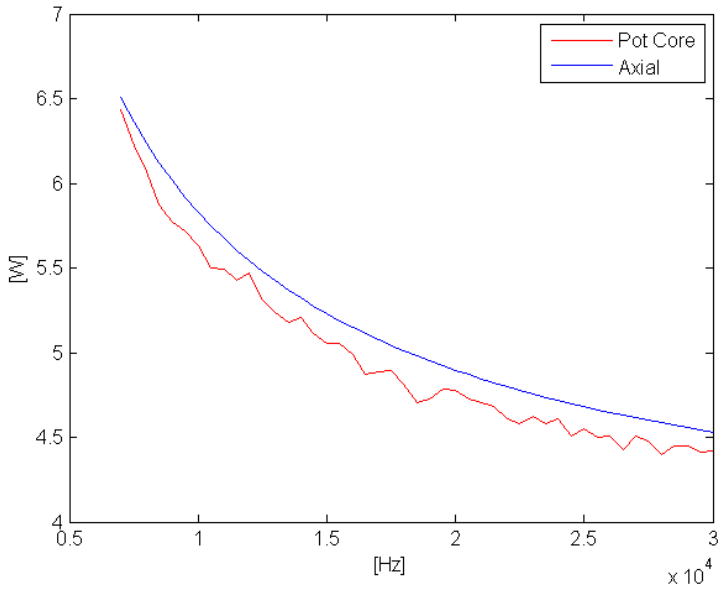

Figure 4.10: Joule Losses vs. frequency.

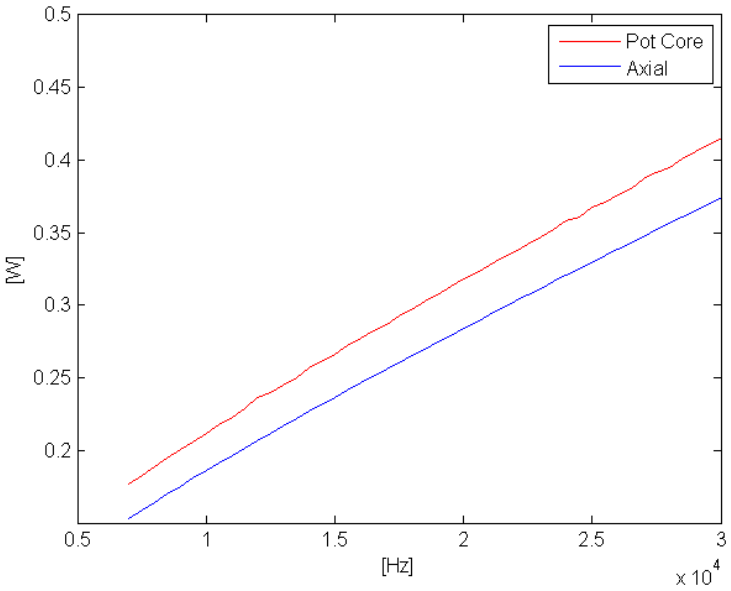

Figure 4.11: Iron Losses vs. frequency.

It is important to say that iron losses in the ferrite and resistive losses in the conductors, are the only losses considered here for the transformers. In fact, eddy currents are not considered in the ferrite core, because the ferrite used is a *soft*

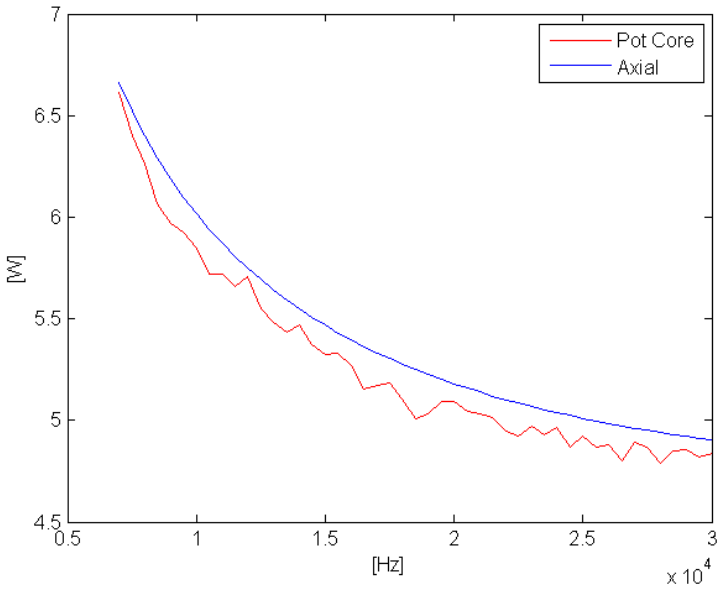

Figure 4.12: Total Losses vs. frequency.

magnetic composite. On the other hand, the skin effect on the conductors due the high frequency, is taken into account only as a reduction in the conductors' cross sectional area.

For the sake of simplicity, this is also done in the FEA, resulting in a higher current density in the wires.

Since the optimization's fitness function is the volume, we can see the volume of both transformers varying with frequency in fig. 4.13.

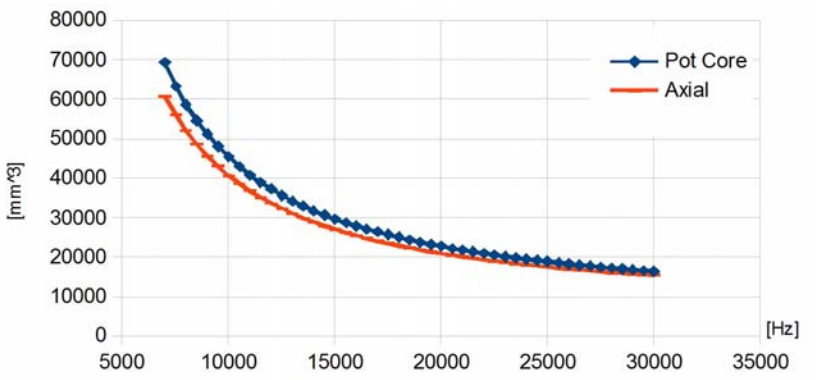

Figure 4.13: Volume vs. frequency.

Effect of the air gap

A peculiar and inherent feature of a rotary transformer is the air gap. Even if it is indispensable for the rotation of the system, the air gap has a high impact on the magnetic properties of the transformer. In particular, it seriously influences the values of the inductances.

In order to see these effects, we vary the air gap value from 0.6 mm to 1.5 mm, and calculate the leakage and the main inductances as shown in section 4.1.

In fig. 4.14 and 4.15, there are the pot core's and axial's leakage and main inductances, respectively. The leakage inductance grows almost linearly with the

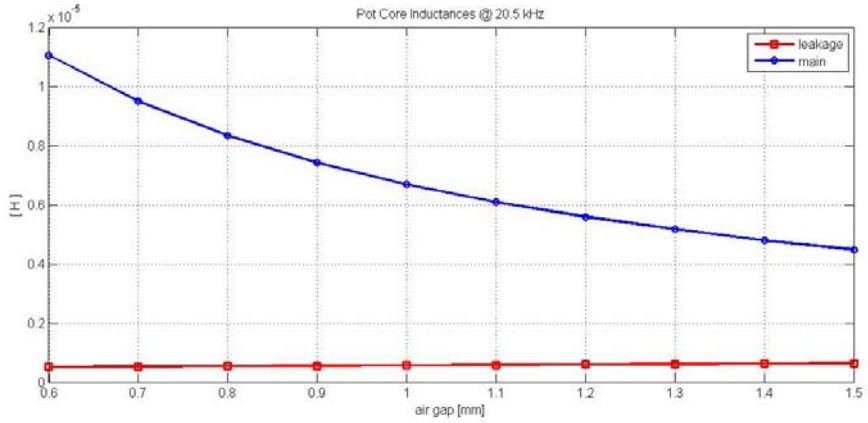

Figure 4.14: Pot core's analytical inductances.

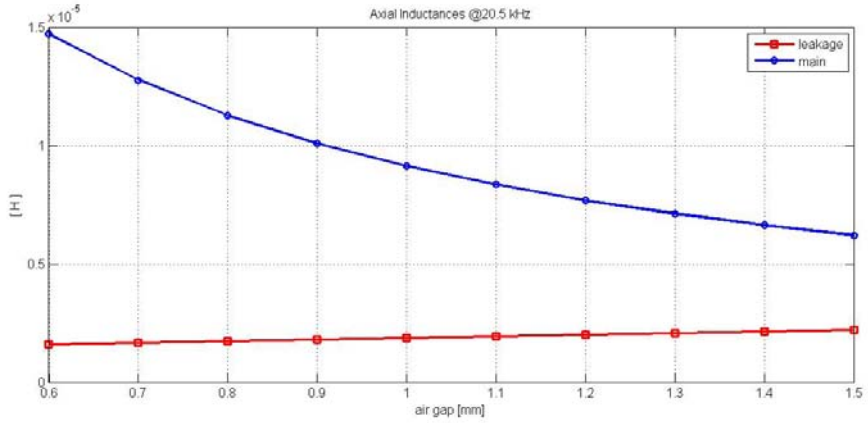

Figure 4.15: Axial's analytical inductances.

air gap length, with a small slope. Ideally increasing the air gap, it would be possible to reach the required value for the ZVT, without adding an external inductance.

But, with the air gap length, the main inductance has a greater drop, meaning high primary currents and hence higher losses. Moreover, an high value of the leakage inductance, leads to higher flux lines lost, and worst magnetic coupling.

So, in order to have the best efficiency in terms of magnetic coupling and low primary currents, it is better to have the smallest feasible air gap length.

Furthermore, it is abandoned in this work the zero voltage transition strategy for the converter.

4.3. Finite Element Analysis

After the optimization of the transformer's geometry, we will now compute a finite element analysis. This step is necessary in order to see the real behavior of the machine. In fact, the analytical analysis of the transformer does not take into account many physical aspects that are instead considered in a FEA.

For instance, we will compute values of the inductances that are closer to the real ones, because in the FEA also the side effects are taken into account. Or we will be able to simulate the full-bridge converter, in order to obtain the actual shape of the currents and of the voltages inside the transformer. And we will therefore compute, not only the efficiency of the transformer, but also the losses on the power electronics's components.

4.3.1. Setting the simulation

In the following pages, we will describe the most important settings for the finite element analysis of the rotary transformer. Even though a particular commercial software has been used [9], we will show the options that could be set for every FEA software of the same level.

Edit application

Since we want to simulate the whole converter, the only possible kind of application is the *Transient Magnetic*. In fact, the driving commands for the full-bridge switches are time dependent.

It is then a $2D$ problem with axial symmetry. The formulation used by default is the *vector model* ($\vec{A}$, V); where $\vec{A}$ is the magnetic vector potential, and V is the electric scalar potential. The definition of this two quantities is

$$\begin{cases} \vec{E} = -\nabla V \\ \vec{B} = \nabla \times \vec{A}. \end{cases} \tag{4.27}$$

Assuming an axial symmetry, we define a reference system (r, z, ϑ). In this system, the magnetic field varies on the plane (r, z), while the current field varies along ϑ. Therefore, referring to the equations (4.27) and the Maxwell equations, it results:

$$\begin{cases} \vec{B} = (B_r, B_z, 0), \\ \vec{A} = (0, 0, A_\vartheta), \\ \vec{J} = (0, 0, J_\vartheta). \end{cases} \tag{4.28}$$

All the fields depend only on (r, z): $B_r = B_r(r, z)$, $B_z = B_z(r, z)$, $A_\vartheta = A_\vartheta(r, z)$, $J_\vartheta = J_\vartheta(r, z)$.

Geometry

We set geometrical parameters in order to simplify the construction of the transformer, and to allow to vary them if needed. The geometrical parameters for both transformers are depicted in fig. 4.16.

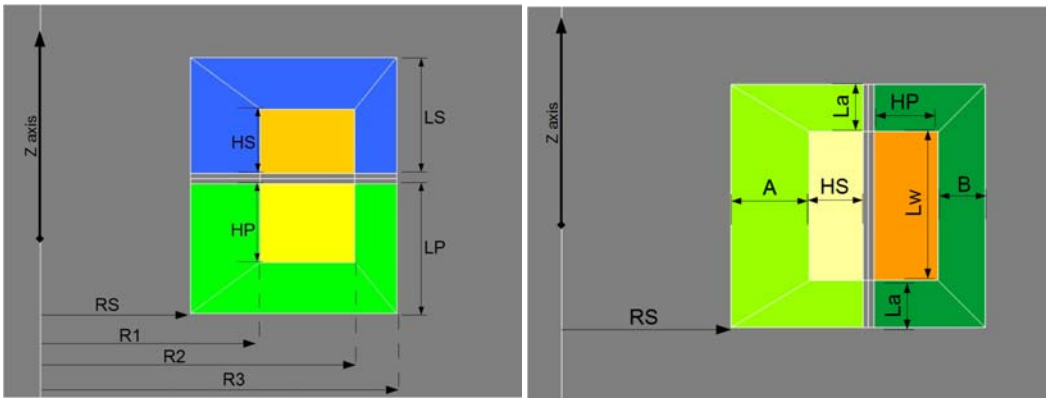

(a) Pot core geometrical parameters. (b) Axial geometrical parameters.

Figure 4.16: Geometrical parametrization for the FEA.

Particular attention has to be paid to the conductor's diameter, because of the skin effect. With a frequency of 20.5 kHz, the copper has a skin depth of about 0.5 mm:

$$\delta = \sqrt{\frac{2\rho}{\omega\mu}}.$$

Since the aim of this work is not to provide a *ready to produce* design, but rather to discuss the general behavior of a rotary transformer, we consider the skin depth effect only as a rise of resistance in the conductors. In order to increase the re-

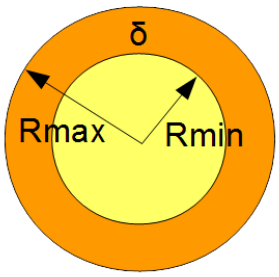

Figure 4.17: Skin effect.

sistance, we use for the wires the diameter d_{eq} equivalent to the area A_{eq} that

represent the skin depth. If δ is the skin dept in [mm]:

$$r_{int} = r_{ext} - \delta \tag{4.29}$$

$$A_{eq} = \pi \cdot (r_{ext}^2 - r_{int}^2) \tag{4.30}$$

$$d_{eq} = \sqrt{\frac{4A_{eq}}{\pi}}. \tag{4.31}$$

That results in a reduced diameter, for instance from 1.6 mm to 1.48 mm.

Materials and components

For the simulation purposes, we use some real materials and components, in order to set the materials for the regions and the electronic components for the circuit editor. The characteristics of these settings are shown in Appendix A.

Electric circuit

In order to set, for each step of the simulation, the sources of the fields inside the geometrical domain, it is possible to represent the electrical circuit of the application. In this way, we can link the elements in the circuit with their respective regions in the geometry.

In fact, for every solution, are necessary the conditions of the boundaries (the characteristics of the potential on the lines of the boundary) and the initial conditions. The latter are given by the electric circuit.

In our application, since we do not know the value of the currents and of the voltages at the transformer's terminals, it is useful to build in the circuit's editor the whole full-bridge converter. The representation of that, can be seen in fig. 4.18; this is the same circuit of fig. 3.3.

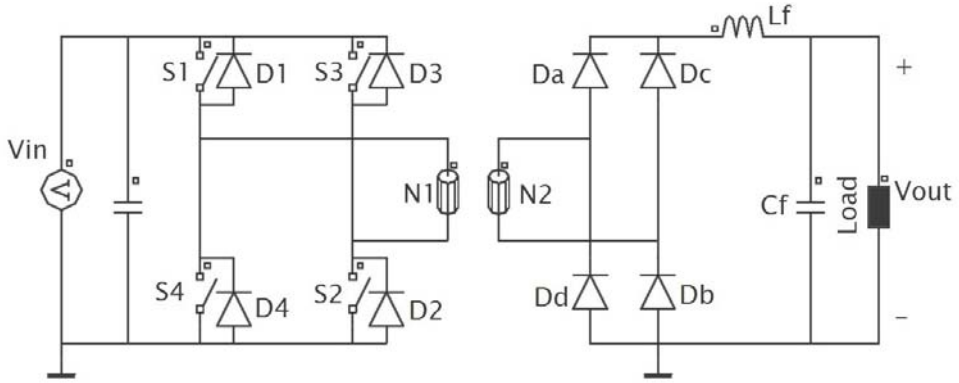

Figure 4.18: Circuit representation in the FEA software.

Referring to circuit 4.18, the connection between the circuit and the geometry context is achieved through the two coupled coils N_1 and N_2. They are the primary side and the secondary side of the transformer, respectively. They are *stranded coil conductors*, and not *solid conductors*, because we consider the skin effect only as an increase of resistance. For the same reason the core's regions are *not conducting regions*, because we use a ferrite and the eddy currents are thus negligible.

This coils in the circuit's editor are then assigned to the regions corresponding to the coils in the geometry context. They are characterized through: the material (copper), the fill factor ($k_f = 0.45$), the number of turns (N_1 or N_2), the orientation of the current, and the equivalent resistance of each coil.

This resistance is defined with parameters, physical or geometrical, so that it can be updated every time some feature of the geometry changes. For instance, for the pot core, the resistance of a coil is:

$$\begin{aligned} R_{coil} &= N_{turns} \cdot \rho \cdot \frac{l}{A} = \\ &= N_{turns} \cdot 1000 \cdot \rho_{Cu}^{100} \cdot \pi(R1 + R2) \cdot \left(\frac{1}{\frac{\pi d_{wire}^2}{4}} \right). \end{aligned} \tag{4.32}$$

The resistivity is considered at 100°C and it is in $[\Omega \cdot \mathrm{m}]$. The geometrical parameters are in mm and they refer to fig. 4.16a. d_{wire} is the diameter of a single wire in [mm].

Driving the switches The four switches in the circuit are *ideal switches*. However, as it is possible to see in Appendix A, they are characterized through the on-state and off-stare resistances, in order to consider the conduction losses.

This switches then, need a *turn-on command*. To implement the switching strategy in fig. 3.4, it has been used the function *valid*.

$$valid(x, x_1, x_2) = 1 \text{ if } x_1 \leq x < x_2, = 0 \text{ else.} \tag{4.33}$$

Whenever the switch has a turn-on command greater than zero, it closes. In our simulation, the function $x = TIME$, and the functions x_1 and x_2 are dependent on the duty cycle and on the frequency, parametrized.

The L-C output filter To smooth the rectifier output voltage and current, it is common to use a L-C filter.

The value needed for the inductance, can be found with the equation (3.11) in section 3.2. We used a $\Delta i_L = 0.2 I_{out}$. The more demanding situation for the filter is for the maximum input voltage, thus for the minimum duty cycle. We obtain:

$$L_f = 0.001 \text{ H}. \tag{4.34}$$

The value of the filter capacitance can be found through the fundamental law of a capacitance:

$$C = \frac{i_C}{\frac{dv_C}{dt}}. \tag{4.35}$$

In this case, $dt = t_{on} = pulse\ duration$, and equation (4.35) becomes:

$$C = \frac{\Delta i_C \cdot I_{out}}{\frac{\Delta v_C \cdot V_{out}}{t_{on}}}. \tag{4.36}$$

We remember that $t_{on} = D/f$, and impose $\Delta v_C = \Delta i_C$. For the capacitance, we consider the maximum duty cycle and obtain:

$$C_f = 0.0000114 \text{ F}. \tag{4.37}$$

4.3.2. Optimized geometry simulations

The first step of the finite element analysis is to simulate the geometry that is found with the optimization. In this way we can compare the analytical results with the FEA results; it is possible to see then if there is enough power transfer, and if the transformer's core saturates. It is important to check also the currents and the voltages across the components of the circuit and see the overall working of the transformer.

Referring to fig. 4.16, the first simulations done have the geometrical characteristics listed in the table below. For both transformers it is important to simulate firstly the working conditions with the minimum voltage of the battery, and thus with the maximum duty cycle, $D_{max} = 0.43$. The frequency is equal to 20500 Hz. For both transformers the radius of the shaft is always $r_S = 9$ mm and the number of primary and secondary turns is $N_1 = 6$ and $N_2 = 5$.

The simulation is a transient, time dependent, and it lasts ten periods of the full bridge working cycle; for a frequency of 20.5 kHz, it corresponds to 0.0004878 s. In fig. 4.19 and 4.20, are depicted the output of the finite element analysis for the optimized geometries of the pot core and the axial transformer. In particular, we can see the magnetic flux density and the flux lines, for the maximum current in the coils.

Pot core	[mm]	Axial	[mm]
HP	4.70	A	4.17
HS	3.90	B	2.50
LP	7.80	HP	3.40
LS	7.00	HS	2.83
R_1	13.20	L_a	2.50
R_2	18.90	L_w	7.90
R_3	21.40		

Table 4.2

The first result is to see that the magnetic core, with the cross sectional area computed from the optimization, does not saturate. Therefore the iron losses will be low.

Secondly, it is interesting to see the different paths that the flux lines take . In fact, many of them are dispersed in the air surrounding the transformer, and the side effects are evident. Consequently, the leakage inductance computed analytically will not be precise.

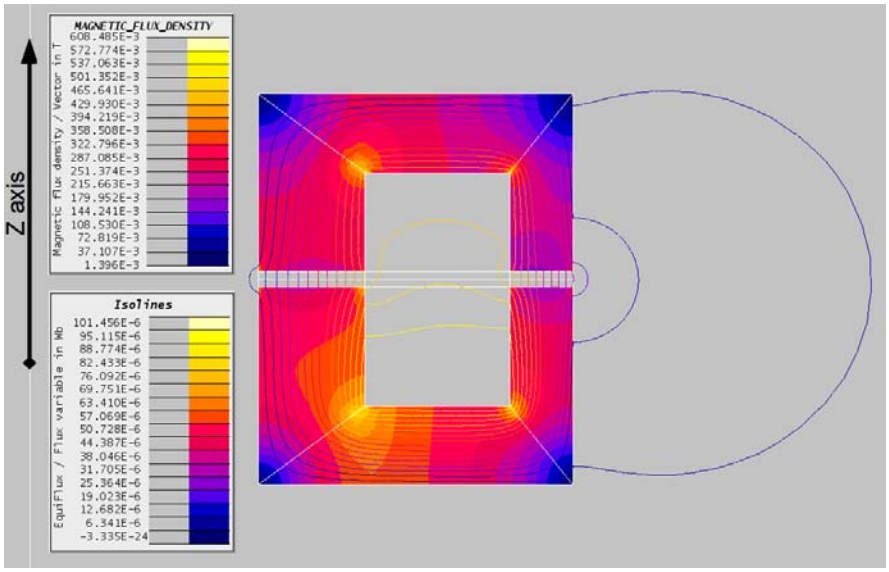

Figure 4.19: Finite element analysis for the optimal pot core.

After these preliminary considerations, we see the voltage and current on the resistance representing the motor, in order to check if there is enough power transfer. As reported previously, the line current that is needed for the rotor, is $I_{out} = 16.24$ A, corresponding to an output active power of $P_{rotor} \simeq 477$ W.

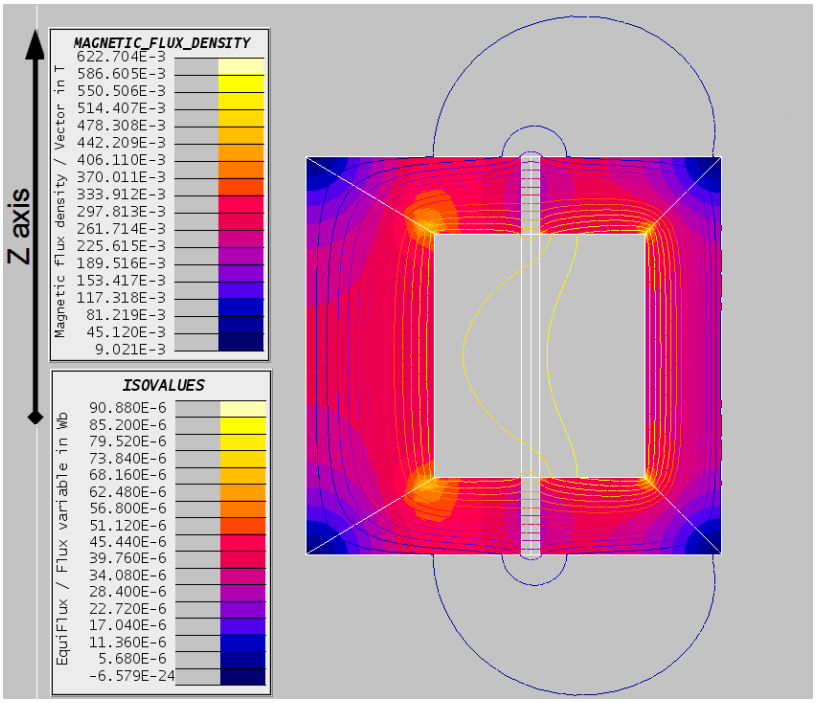

Figure 4.20: Finite element analysis for the optimal axial.

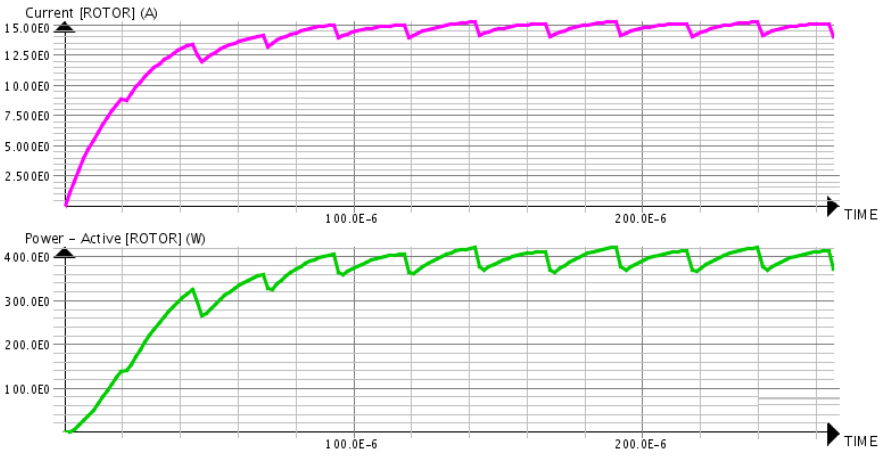

Figure 4.21: Output power of the pot core from the optimization.

From fig. 4.21, we can see that, for the pot core coming from the optimization, there is not enough current for the correct working of the motor. More precisely, the output mean current for the pot core is equal to 14.80 A. For the axial rotary transformer we have a similar result, with a $I_{out} = 15.79$ A. In fig. 4.21, the output has a L-C filter with a bigger Δi_{out} in order to see better the time periods.

This behavior can be explained with the presence of the air gap. In fact, with an air gap inside the magnetic path, the flux lines have a leakage component. This leads to a relatively big leakage inductance, which causes a voltage drop across the transformer's windings. Consequently, the working law of the full-bridge converter expressed in equation (3.7) is not longer valid. It must take into account this impaired voltage gain.

4.3.3. Comparison between analytical and FEA results

Before going further with the design of the transformers, it is important to make a comparison between the results found in the FEA and the analytical considerations that were made before the optimization. In particular, it is interesting to compare the inductances.

Analytically, we computed the main and the leakage inductances with a variation of the air gap's length. With many simulations with the transformer's terminals opened, and following the procedure described in section 4.1, we find the self inductances L_1 and L_2, the mutual inductance M, for each value of the air gap (from 0.6 mm to 1.5 mm). With these values, we use the equations (4.5), and we can make the fig. 4.22 and fig. 4.23.

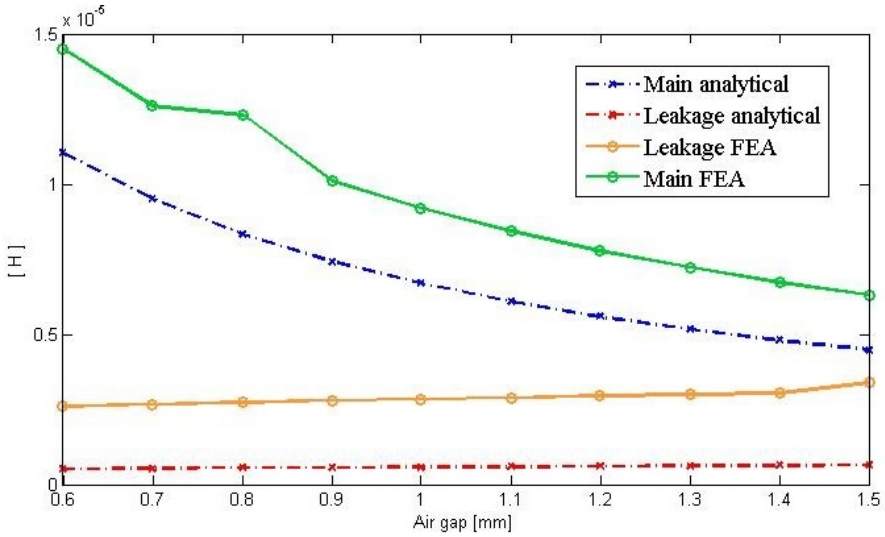

Figure 4.22: L_{lk} and L_m, with a variation of g, for the pot core.

It is important to say that, since the magnetic flux density in the ferrite core is always below the saturation value, the inductances are constant and they do not vary with the current.

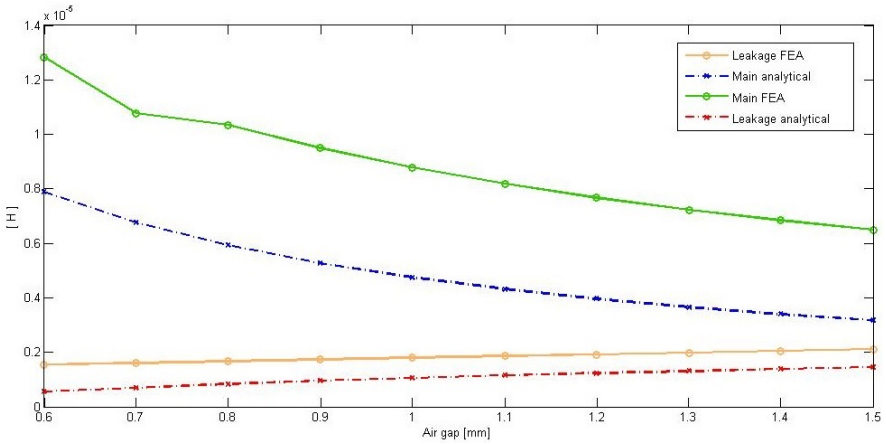

Figure 4.23: L_{lk} and L_m, with a variation of g, for the axial.

The main inductance is higher for the smaller air gap and it has a considerable drop with the increase of the air gap's length. On the contrary, the leakage inductance has a small, almost linear, rise with the air gap.

Therefore, looking at these pictures, we can conclude that:

- since small main inductances and big leakage inductances influence negatively the behavior of the transformers, it is always better to have the air gap's length as small as possible. The losses on the primary side will be reduced, and the power transfer improves.
- the analytical expressions are not precise, but they can be used in the first steps of the design in order to see the behavior of the inductances, at the variation of some parameters.

4.3.4. Degrees of freedom in the design

In the subsection 4.3.2, we see that the transformers coming from the first optimized design do not have the expected power transfer because of the presence of the leakage inductance.

In order to achieve the desired power transfer, thus the rated output current on the rotor, we look at the power transfer expression for a transformer:

$$P_T = \frac{\sqrt{2}\pi}{2} \cdot f \cdot A_c \cdot A_{Cu} \cdot B_{max} \cdot J. \tag{4.38}$$

The factors that affect the power transfer are many, but only a few are viable in this particular case. In fact, we do not want to increase the size of the transformer, and thus the area of the core A_c nor the area of the copper A_{Cu}. The current density

J is already almost the maximum possible. Finally there are the frequency and the flux density.

In order to see better the relationships between these factors, we remember the expression of the maximum flux density for the full-bridge converter:

$$B_{max} = \frac{V_{in} \cdot D}{2 \cdot N_1 \cdot f \cdot A_c} = \frac{V_{in} \cdot t_{on}}{2 \cdot N_1 \cdot A_c}. \tag{4.39}$$

If only the frequency changes, the pulse duration for each period $t_{on} = D/f$ will decrease accordingly. For the same duty cycle D, the change of the frequency will not affect the power transfer.

If we consider also the full-bridge fundamental relationship

$$V_{out} = 2\frac{N_2}{N_1} \cdot D \cdot V_{in} \tag{4.40}$$

there are two possibilities to increase the power transfer, or, equivalently, to increase the output voltage. We can:

1. decrease the number of primary coils N_1,
2. decrease the ratio $n = N_1/N_2$ of the transformer.

Two possibilities are considered:

$$\begin{cases} n = 1.1 \rightarrow N_1 = 11,\ N_2 = 10 \\ n = 1.0 \rightarrow N_1 = 5,\ N_2 = 5 \end{cases}$$

The first possibility, $n = 1.1$, does not work. In fact, with the maximum duty cycle of 0.43, the output current is still not enough: $I_{out} = 14.85$ A. On the contrary, it is even less than the first attempt with $N_1 = 6$ and $N_2 = 5$.

The explanation is pretty simple. Even if the ratio n decreases, the number of primary coils N_1 increases. Thus the flux density decreases. Moreover, both leakage inductance and main inductance are directly proportional to N_1^2; the increase of the leakage inductance leads to an impaired voltage gain.

The solution that leads us to two working transformers is the one with $N_1 = 5$ and $N_2 = 5$.

4.3.5. Two working rotary transformers

We do first a FE simulation with $n = 1$ and the same geometries coming from the optimization; see table 4.2 and fig. 4.19 and 4.20.

The first important result is that with the number of turns equal to $N_1 = 5$ and $N_2 = 5$, and the maximum duty cycle $D = 0.43$, we have enough power transfer for both pot core and axial transformer.

	Pot core	Axial
I_{out}	17.81 A	16.60 A

So, there is also more than the needed current for the maximum duty cycle; this means that there is the possibility to give more current on the rotor if it will be necessary, and that the correct maximum duty cycle that gives $I_{out} = 16.24$ A is less than the limit (that we set) of 0.43.

There is a problem though, that makes these geometries unfeasible. In fact, the *rms* current density in the primary side is always more than 10 $\mathrm{A/mm^2}$, for both pot core and axial: respectively we have $J_1 = 16.48$ $\mathrm{A/mm^2}$ and $J_1 = 19.34$ $\mathrm{A/mm^2}$.

The cause can be found in the small values of the main inductance, that recalls a big amount of magnetizing current on the primary side. In fact, the current density's limit is not respected only on the primary side, even though the ratio is unitary and the diameter of the primary and of the secondary wires is the same.

There is the need so to use bigger wires only on the primary side, anyhow respecting the geometric constraints. We modify the geometry of the transformers, so that the current density is less or equal to 10 $\mathrm{A/mm^2}$. The fill factor is always the same and the size of the slots is changed in such a way that the overall axial length is minimal. Always referring to fig. 4.16, the geometrical parameters of the final working transformers are listed in the table below.

Pot core	[mm]	Axial	[mm]
HP	4.80	A	4.17
HS	2.30	B	2.50
LP	7.90	HP	6.90
LS	5.40	HS	2.83
R_1	13.20	L_a	2.50
R_2	22.83	L_w	8.00
R_3	25.33		

The diameters of the primary wires that has been used are equal to 2.3 mm for the pot core and 2.5 mm for the axial. If we keep into account the skin effect for

20.5 kHz, the equivalent diameters are 1.9 mm for the pot core and 2.0 mm for the axial.

As we did for the optimal geometries, we represent in fig. 4.24 and 4.25 the post processed geometries, with flux lines and magnetic flux density.

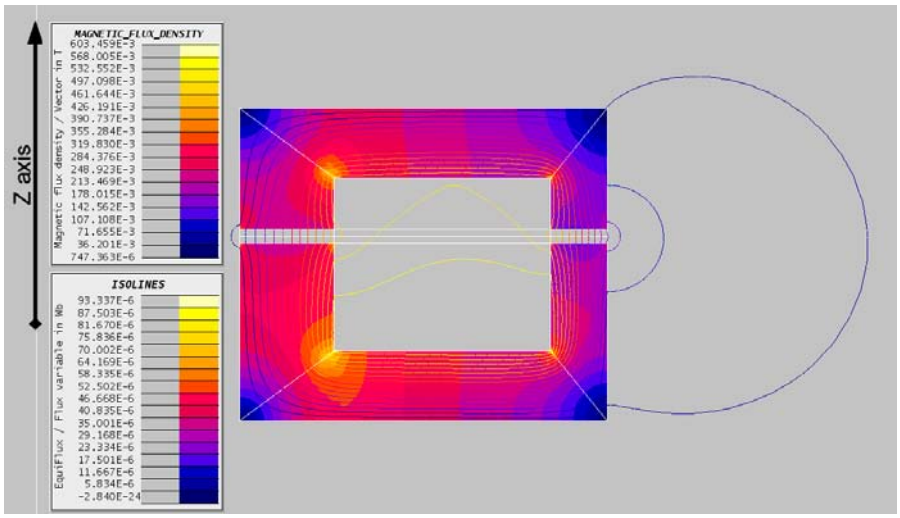

Figure 4.24: Finite element analysis for the working pot core.

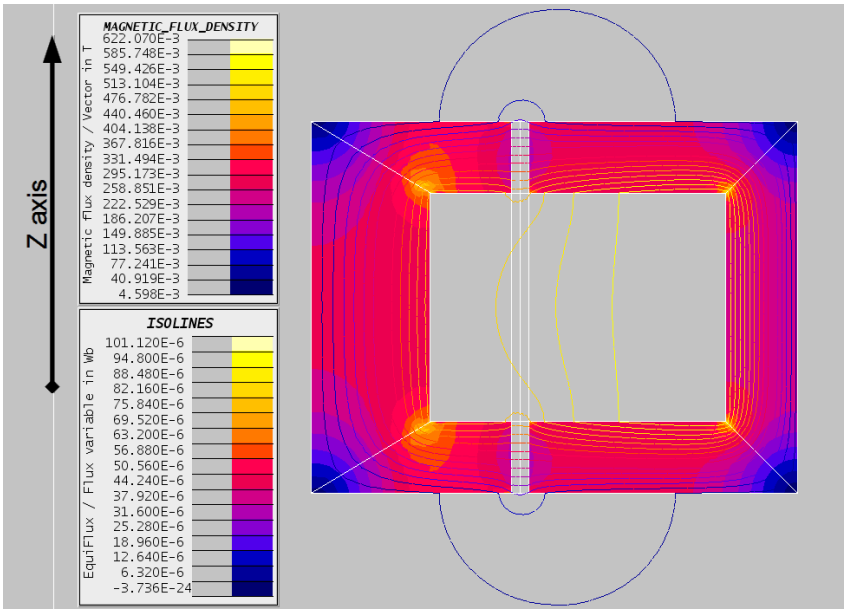

Figure 4.25: Finite element analysis for the working axial.

The results of this last modification of the transformers lead to a pot core and

an axial transformer, that are fit for the application of this work and that could be taken to the construction's stage.

In the following table there are some characteristics of the final transformers that are taken from the post processing of the FEA.

	minimum V_{in}		maximum V_{in}	
	pot core	axial	pot core	axial
D	0.315	0.31	0.23	0.24
I_{out}	16.57 A	16.34 A	16.11 A	16.66 A
I_1^{rms}	26.41 A	32.68 A	23.32 A	29.54 A
I_2^{rms}	16.57 A	16.33 A	16.11 A	16.68 A
J_1	9.30 A/mm^2	10.43 A/mm^2	8.21 A/mm^2	9.41 A/mm^2
J_2	9.65 A/mm^2	9.49 A/mm^2	9.14 A/mm^2	9.70 A/mm^2

Looking at these values, we see that the maximum duty cycle is more or less equal to 31%, for both transformers. The exact value of the duty cycle for every working condition is achieved through a closed loop control on the rotor current.

The fact that the maximum duty cycle is less than the ideal maximum is a positive occurrence. In fact, in the real motor, the current needed in the rotor's conductors is more than the ideal. The magnetic field of the rotor is indeed influenced by the rotating field of the stator. As we see in fig. 4.26, the d component of the stator field is opposite to the rotor field: consequently, in order to achieve the same torque, the current in the rotor must increase its value. This is possible with an increase of the duty cycle of the converter.

However, an increase of the rotor current means an increase of the resistive losses on the rotor of the machine.

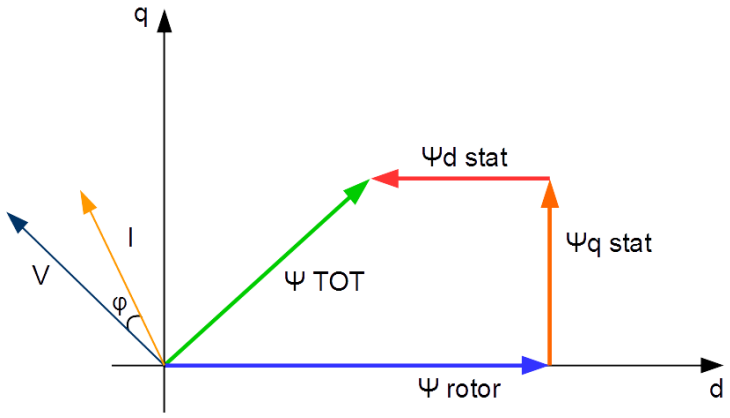

Figure 4.26: Qualitative phasorial representation of the motor's fluxes [11].

Comparison of the results

Lastly, in order to make a final comparison between the pot core rotary transformer and the axial rotary transformer, we compute the losses and the efficiency of the transformers and of the whole converter, and we also compute the inductances.

The efficiency is computed as the ratio between the *rms* value of the output power and the *rms* value of the input power. But to consider also the iron losses computed analytically, we subtract them to the output power:

$$\eta_{transf} = \frac{P_{out} - P_{hy}}{P_{in}}. \tag{4.41}$$

These results are shown in table 4.3.

		pot core	axial
Joule losses	P_J	4.94 W	4.72 W
Iron Losses	P_{iron}	0.019 W	0.098 W
Transformer's efficiency	η_{transf}	98.9%	99.2%
Total Efficiency	η_{TOT}	67.35%	61.10%
Leakage inductance	L_{lk}	$1.060 \cdot 10^{-6}$ H	$9.47 \cdot 10^{-7}$ H
Magnetizing inductance	L_m	$1.149 \cdot 10^{-5}$ H	$8.82 \cdot 10^{-6}$ H
Primary current	I_1^{rms}	24.9 A	31.2 A
Secondary current	I_2^{rms}	16.2 A	16.5 A
Diameter primary conductors	d_{c1}	2.3 mm	2.5 mm
Diameter secondary conductors	d_{c2}	1.6 mm	1.6 mm

Table 4.3: Final comparison between pot core and axial.

The resistive losses are computed through the FEA post-processing and they are similar for the two kinds of transformer because the coils are almost the same, as well as the diameters and the current densities.

The losses in the ferrite are computed through the Steinmetz simplified expression (see Appendix A). They are very low because of the small volume and the particular ferrite used. Moreover, the magnetic flux density is not constant and it is far from the saturation value. The value in [T] that is needed to compute the iron losses is taken from the post-processing:

- we want the mean value of B in a period,
- we evaluate for every time step the value of $\iint mod(\vec{B})dA$ onto the area that represent the section of the ferrite core,

- we finally divide the *rms* value of this for the area on which it was calculated.

The efficiencies of the only transformers are really high, and they are similar and around the 99%. This efficiency is more than the efficiency of a slip and brushes system, that is roughly around 90%. But we must keep in mind that the thermal losses are not considered here.

Unfortunately, the efficiency of the whole converter is dramatically lower than the transformer's, and lower than the efficiency of the slip rings system. In fact, the whole converters have a mean efficiency of 64%; this means that the 98% of the losses are due to the converter, and not to the transformer.

We also see that the pot core efficiency of $\approx 67\%$ is better than the axial efficiency of $\approx 61\%$, even if the axial transformer has less losses than the pot core. This can be explained looking at the primary currents and the main inductances. In fact, the losses of the converter are mostly losses of the full-bridge inverter, respectively conduction losses and commutation losses on the switches. A smaller value of the axial main inductance leads to higher magnetizing currents for this transformer.

The smaller main inductance is also the cause of the different diameters of the primary wires for the two transformers. Because of this small L_m, the axial transformer needs bigger primary conductors than the pot core transformer. This leads also to a bigger volume for the axial transformer, that becomes now almost equal to the pot core in terms of size.

So all in all, the pot core rotary transformer that is designed in this work is better than the axial rotary transformer, and both of them could be built for a real motor.

4.3.6. Effects of the inductances

In this work, we saw that the peculiar feature of these transformers, the air gap, has a huge influence on the behavior of the transformer itself, and of the whole system. In particular, the major effects are due to the not conventional inductances.

Besides the effects on the efficiency and on the geometry that we have already seen in the previous section, there are still two effects that are worth to be mentioned. In fact, they affect mainly the converter behavior, which is the responsible for the efficiency of the whole converter.

The first noticeable phenomenon concern the free wheeling period of the diodes of the full-bridge. These diodes are placed in anti-parallel to the switches, in order to let flow the current that is still stored in the transformer when the switches are all opened. Usually, this free-wheeling transition is almost negligible. In our case however, this period is much longer because the presence of the big leakage inductance.

As a consequence, when all the switches are off, the current flows back to the source, as we can see in fig. 4.27.

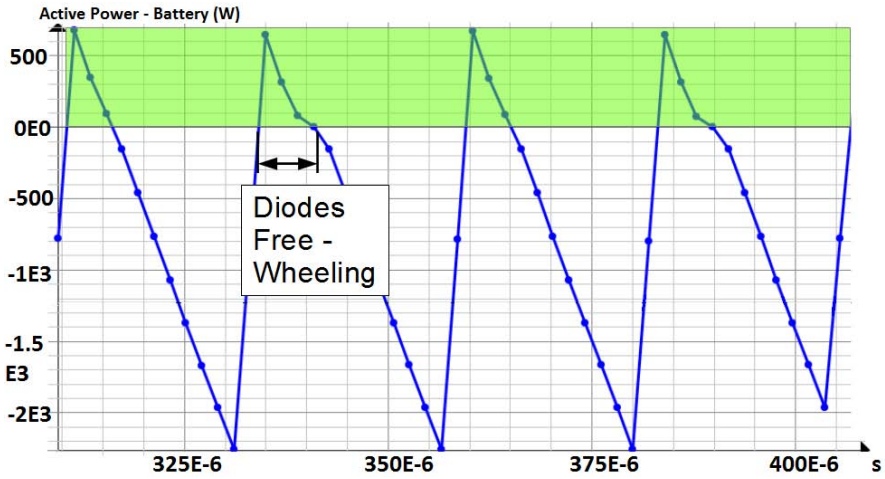

Figure 4.27: Active power in [W] of the voltage source.

During the free wheeling of the diodes so, the current keeps flowing in the transformer's primary: the power transfer period is therefore longer than the ideal.

This leads us to the second effect of the inductances. In fact, this long free wheeling duration affect also the voltage on the primary side of the transformer, which is far from the ideal wave shown in fig. 3.4.

In order to explain this phenomenon, we refer to fig. 4.28. The first lines are the turn-on commands of the switches. The blue signal is the on-state function for the diagonal leg composed by switches $T1$ and $T2$; the pink one is for the other diagonal leg composed by switches $T3$ and $T4$.

Secondly there is the current across switch $T1$ and diode $D3$. For switch $T3$ and diode $D1$ the currents are the same, with a delay of half a period T. Note that the currents, voltages, and drives, are the same for switches $T1$ and $T2$, and for switches $T3$ and $T4$, as well as for the couples of diodes $D3$ and $D4$, and for diodes $D1$ and $D2$. For instance, in fig. 4.28 is depicted the current of switch $T1$; we have the same current for the switch $T2$. When these switches open, the diodes $D3$ and $D4$ begin their free wheeling period. This is why it is enough to represent only the currents i_{S1} for $T1$ and current i_{D3} for the diode $D3$.

Therefore, when all the switches are open, the voltage v_1 does not fall to zero, as in the ideal case, but it goes to the voltage battery again (with the opposite sign). This happens because, when the switches $T1$ and $T2$ are opened, the current i_1 is not zero because of the inductances, and it keeps flowing through diodes $D3$ and $D4$. The primary side of the transformer result thus still connected to the battery. When finally the current falls to zero, also the voltage on the transformer goes

almost to zero (there is still the reflected secondary voltage.)

The overall effect of this, is an “extended duty cycle”. Since the voltage v_1 is different from zero for a longer period of time than expected, the mean value of the voltage that will be transferred to the load will be higher.

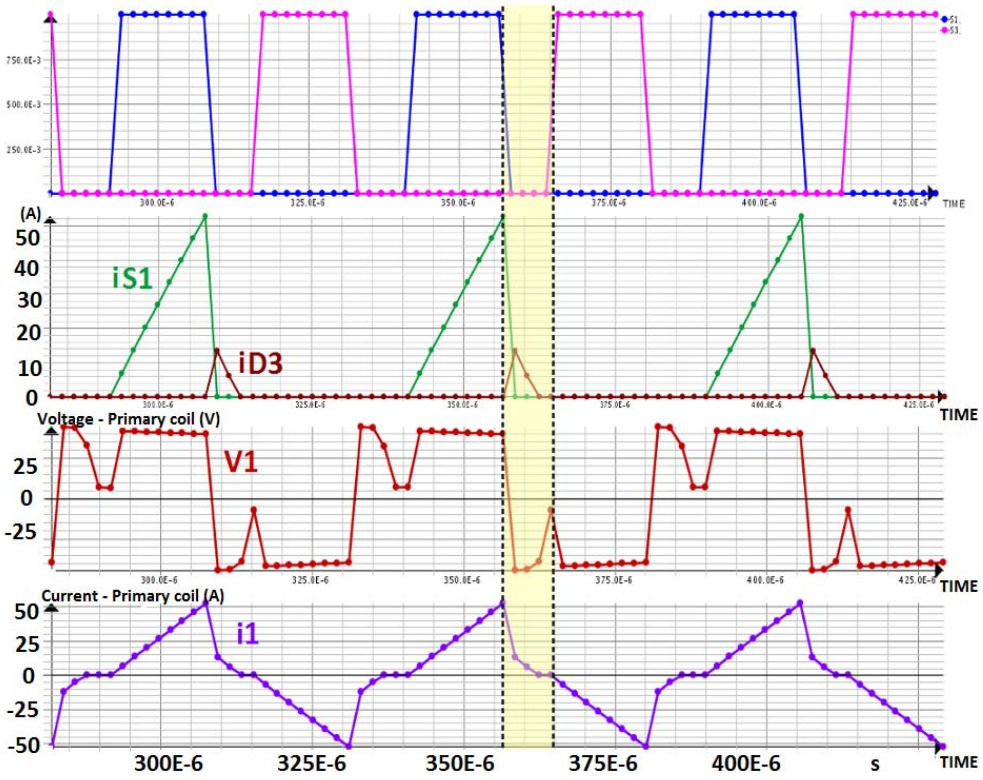

Figure 4.28: Effect of the inductances on the duty cycle.

4.3.7. Dynamic of the load

Finally, it is important to make a comparison in terms of dynamic behavior of the rotary transformer with the typical dynamics of the slip and rings system.

Firstly, we do not find in this work the exact duty cycle for every input voltage. And we do not consider either the effect of the stator flux on the request of output current. For the latter issue, we already said that there is probably enough duty cycle’s range to have more current whenever is needed. On the other hand, the control of the duty cycle is done through a close loop control on the rotor current.

The last phenomenon to analyze is the transient. For the slip and brushes system the leading factor in the transient is the inductance of the rotor winding or the inductance of the filter. As we can see in fig. 4.29, for the rotary transformer it happens the same.

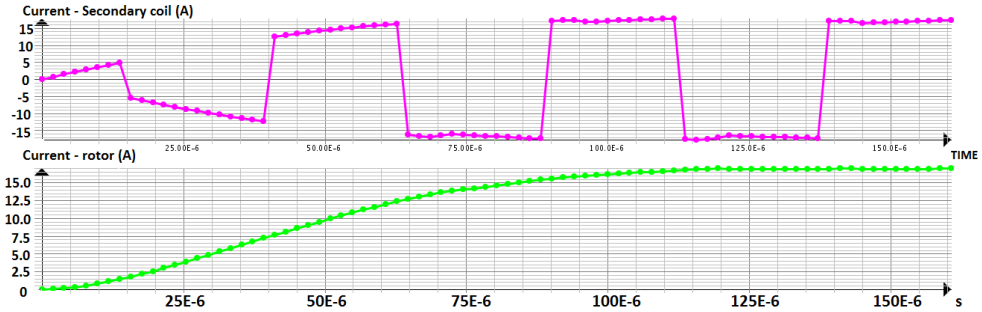

Figure 4.29: Transients of the transformer and of the rotor.

We do not simulate the closed loop control of the current, nor the inductance of the rotor, because we do not know all the characteristics of the real motor and because this thesis wants to illustrate the general behavior of a rotary transformer.

In this way it is possible to design the proper rotary transformer also for other specific applications. For instance, we used a converter that is viable only for a motor: using different and bi-directional converters, it would be possible to implement a rotary transformer system also for a generator.

CHAPTER 5

Conclusions

The two rotary transformers that are designed in this thesis have both fulfilled the request of radial and axial size, and they could be built for the real electrically excited synchronous motor.

However, there are some considerations that are valid for the design of every rotary transformer. Firstly, the leakage inductance and the main inductance are highly significant in the transformer's behavior. The small main inductance leads to high magnetizing currents and thus high primary currents and resistive losses. On the other hand, there is a big leakage inductance that causes a voltage drop on the transformer, which leads to an impaired voltage gain. Moreover, the leakage inductance affects the dynamic of the electronic converter. In order to limit and control these effects, this work gives some important advices:

- the air gap length must be as small as possible,
- in order to reduce the leakage inductance, if possible, use coaxial windings to increase the magnetic coupling,
- remember that both inductances are proportional to N_1^2.

Anyhow, with this kind of electronic converter and for this application, the pot core rotary transformer seems better than the axial. In fact, thanks to the bigger main inductance, the pot core has smaller primary currents, and the overall efficiency (67%) is higher than the efficiency of the axial (61%). Always due to the bigger main inductance, the pot core needs smaller conductors on the primary side; consequently, the volumes are now similar, unlike what happened for the analytical design, where the pot core was slightly bigger than the axial.

Therefore, if there are size issues, the rotary transformer is a valid alternative to the brushes and slip rings system. Furthermore, with the rotary transformer it is avoided the wear of the brushes, and the motor with the rotary transformer excitation proves to be more reliable than the conventional electrically excited synchronous motor. In our case then, it is minimized the volume, but many other geometric parameters could be minimized for every specific application.

However, for automotive applications, many other characteristics are requested. The EESM with the rotary transformer, does not use permanent magnets, reducing the overall cost of the machine and avoiding the environmental issues related to the use of rare earth magnets. Respect to a permanent magnet synchronous machine, it has the possibility to control the excitation current, allowing then an optimized mechanical characteristic, for every working condition.

The biggest drawback then, is the overall efficiency. The PMSMs have high efficiencies, while the EESMs with rotary transformers have an additional source of losses on the rotor. On one hand, there is the small main inductance of the rotary transformer, that cause high resistive losses on the transformer primary side. On the other hand, an EESM has resistive losses on the rotor's conductors, where it is more difficult to do a proper thermal cooling. Furthermore, in this work the thermal losses are not considered for the transformer.

In conclusion, the EESM with a rotary transformer is not competitive in terms of efficiency with a PMSM, unless the efficiency of the whole rotary transformer excitation system does not improve. This can be achieved reducing the losses' sources also in other parts of the machine. Since this technology is not yet very experienced, there is still room for improvement. For instance, it could be possible to improve the thermal cooling of rotating parts, like the rotor of an electrically excited synchronous machine, or in specific applications it would be possible to use different kind of converters, exploiting the leakage inductance in order to achieve soft switching.

APPENDIX A

Materials and components

Copper It is used the *copper* inside the materials' database of the finite element analysis software. The copper's resistivity at 20 °C is equal to $\rho_{Cu}^{20} = 0.016\ \Omega\text{mm}^2/\text{m}$.

The temperature chosen for the simulations is $T_1 = 100$ °C, so that the resulting resistivity is:

$$\begin{aligned}\rho_{Cu}^{100} &= \rho_{Cu}^{20} \cdot (1 + \alpha(100 - 20)) = \\ &= 0.016(1 + 0.004(100 - 20)) = 0.02112\ \frac{\Omega \cdot \text{mm}^2}{\text{m}}.\end{aligned} \tag{A.1}$$

MOSFet and diodes For the FEA are implemented four switches and eight diodes, and for the simulation purposes are reported here the inputs needed: the on-state and the off-state resistances. Another characteristic used in the optimization is the output capacitance of the MOSFet, equal to $C_{oss} = 156$ pF.

	$R_{on-state}$	$R_{off-state}$
MOSFet	0.0220 Ω	1 MΩ
Diodes	0.0217 Ω	1 MΩ

Table A.1

For further information, see [6] and [7].

Ferrite and mechanical stresses The characteristics of the ferrite used in this work are listed in table A.2. For further information see [15].

Frequency	$20 \div 750$ kHz
Saturation flux density	530 mT
Initial permeability	$3000 \pm 25\%$
Density	4.8 g/cm^3

Table A.2

The magnetic properties of this ferrite can be seen also in the B-H characteristic in fig. A.1. The curve can be easily found as an *isotropic analytic saturation curve*, given the initial permeability μ_r of the ferrite and the saturation flux density B_{sat}. This kind of curve defines a non-linear $B(H)$ dependance for an isotropic material, taking into account the saturation. The mathematical expression of this curve comprises a straight line plus an arc tangent.

$$B(H) = \mu_0 H + \frac{2B_{sat}}{\pi} \cdot \arctan\left(\frac{\pi(\mu_r - 1)\mu_0 H}{2B_{sat}}\right). \tag{A.2}$$

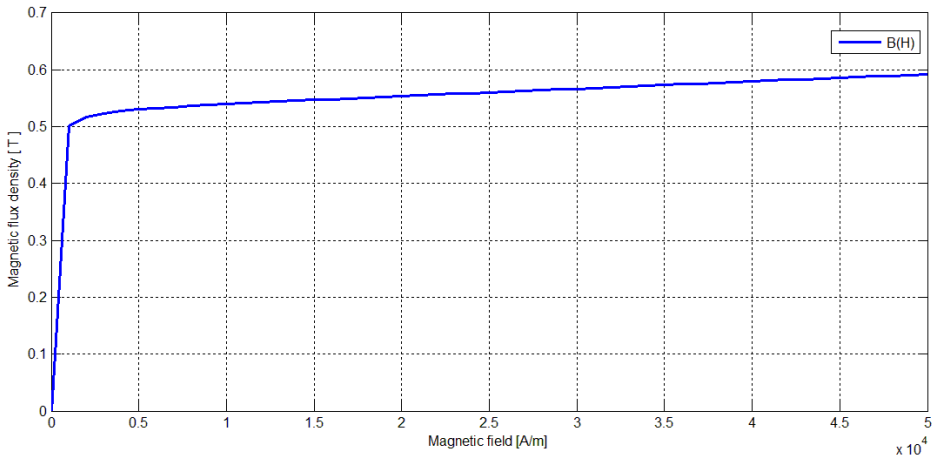

Figure A.1: *T-ferrite* B-H characteristic [15].

This particular ferrite is good for high frequency application because it is a *SMC* and the eddy currents are negligible, and it has very low hysteresis losses (iron losses). The iron losses are computed through the Steinmetz simplified equation:

$$P_{iron} = C(T) \cdot f^{\alpha} \cdot B^{\beta} \cdot Volume. \tag{A.3}$$

where $C(\mathrm{T})$ is a temperature depending constant, at 100°C equal to 3.354 $\mathrm{mW/cm^3}$, α is equal to 1.926 for f in kHz and β to 2.731 for B in Tesla.

In section 4.2.6, it is chosen as minimum core thickness 2.5 mm. This value was obtained looking at different ferrite constructor's datasheets. But this transformers also have a rotational speed, in this case the rated speed is 12000 rpm. So, we do here an easy and simplified mechanical analysis [19] in order to check if the rotational stresses are less than the *ultimate tensile strength*, *UTS*, of the ferrite. For MnZn ferrites, UTS is usually $20 \div 65$ MPa.

We take a cylindrical reference system r,t,l, where r is the radial component and l is the component along the symmetry axis. The tensile strengths are then, σ_r, σ_t, and σ_l. Under this hypothesis:

1. geometry and loads axisymmetric,
2. geometry and loads constant along the axis,
3. σ_l =const,

the tensile strengths depend only on the radius r.

The transformers can be represented as a sum of hollow discs and hollow cylinders. In both these cases, $\sigma_l = 0$, and the tensile strengths are the following. For a hollow disc, with maximum and minimum radius r_2 and r_1, respectively, the strengths are:

$$\sigma_r(r) = (3+\nu)\frac{\rho\omega^2}{8}\left[r_1^2 + r_2^2 - \frac{r_1^2 \cdot r_2^2}{r^2} - r^2\right] \tag{A.4}$$

$$\sigma_t(r) = \frac{\rho\omega^2}{8}\left[(3+\nu)(r_1^2 + r_2^2 + \frac{r_1^2 \cdot r_2^2}{r^2}) - (1+3\nu)r^2\right] \tag{A.5}$$

where

- ω, rotational speed of the object, in rad/s;
- $\rho = 4800\ \mathrm{kg/m^3}$;
- $\nu = 0.28$, Poisson's coefficient.

For a hollow cylinder we have the same expressions as in A.4 and A.5, with $\nu/(1-\nu)$ instead of ν.

If we do solve these expressions for our final geometries, we see that the maximum tensile strengths do not reach the UTS. Fig. A.2 and A.3 depict the strengths for the rotating pot core, while fig. A.4 and A.5 for the rotating axial.

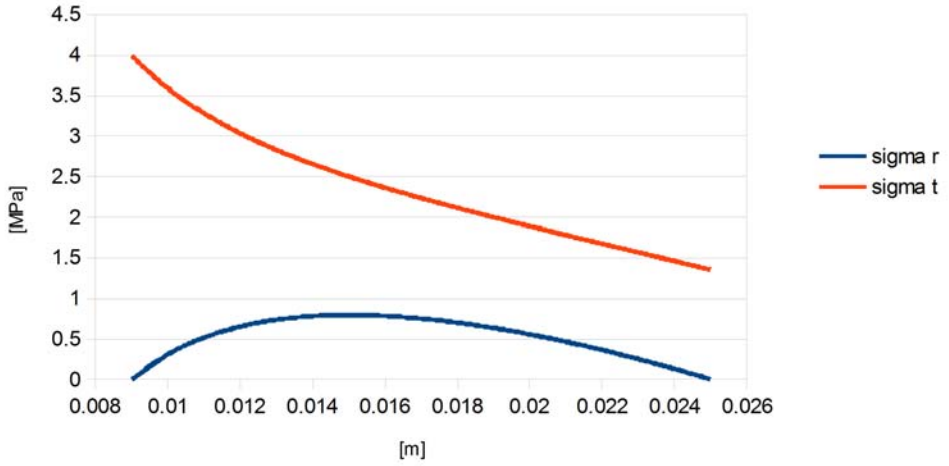

Figure A.2: Pot core as a hollow disc, at 12000 rpm.

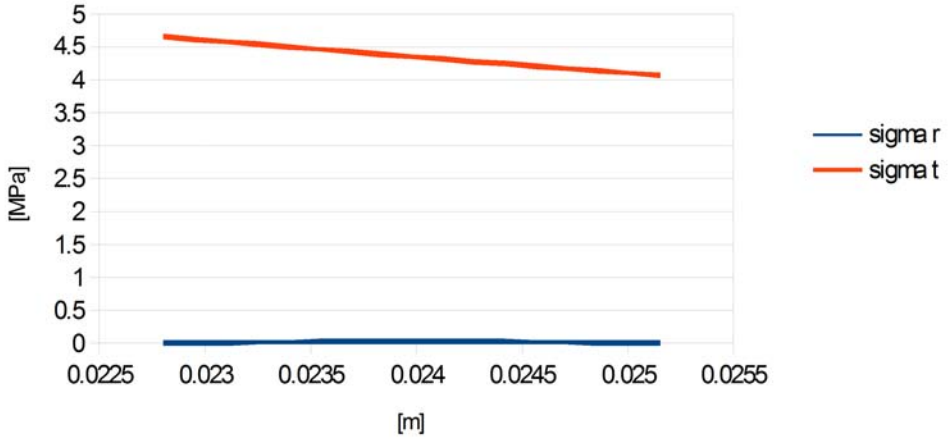

Figure A.3: Pot core as a hollow cylinder, at 12000 rpm.

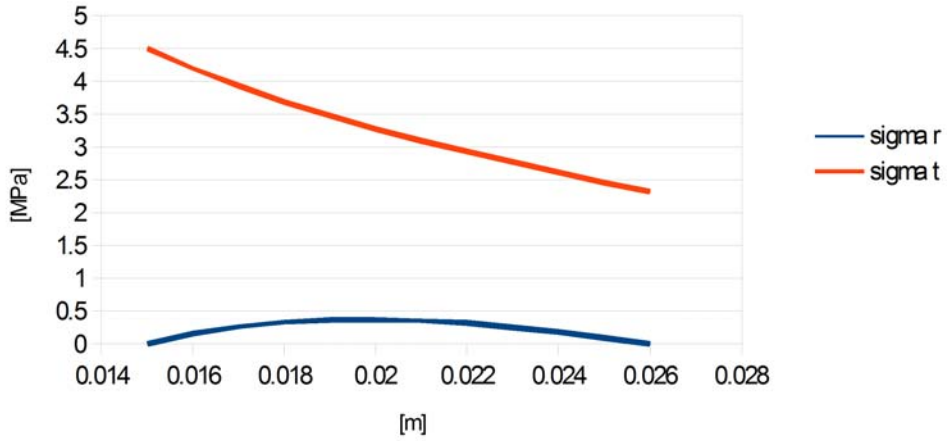

Figure A.4: Axial as a hollow disc, at 12000 rpm.

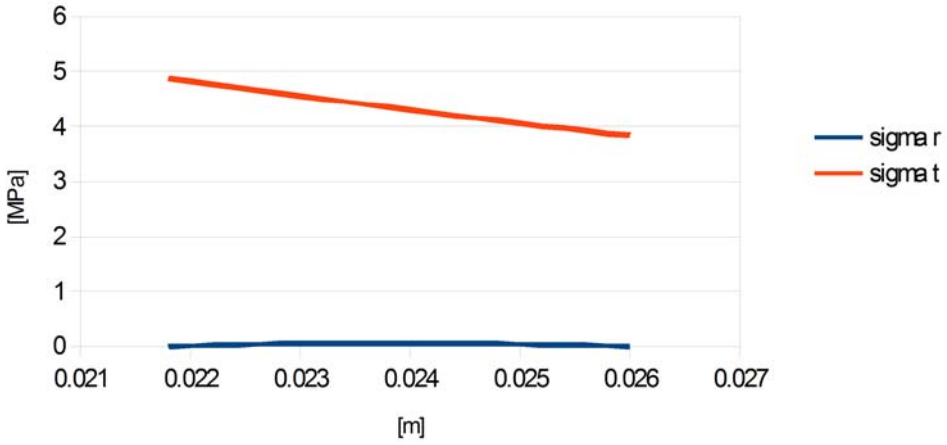

Figure A.5: Axial as a hollow cylinder, at 12000 rpm.

APPENDIX B

Multiobjective Optimization and Weighted Approach

Multiobjective Optimization With the multiobjective optimization genetic algorithm, *gamultiobj*, it is possible to have more than one objective function to minimize. For this work it would be convenient to choose as objective functions the *volume* and the *losses*.

The result of a multiobjective optimization is the *Pareto Front*. The Pareto Front is represented in a plane, where onto the two axis there are the possible values of the two fitness functions. In this plane there are the points representing the values of the two fitness functions, evaluated in some combinations of the optimization's variables.

Usually the two objectives, or the minimum values of the two functions, are in conflict. Therefore there is not a single optimal point or a single set of variables. The Pareto Front represent the different sets of variables that gives equally optimal solutions. The Pareto Front is composed by those points for which there is no point at the same time that it is better for all objectives considered in the optimization function (see fig. B.1).

This method is often used in engineering because, given multiple optimal solutions, the designer can decide the best solution accordingly to her/his project.

With the MATLAB®Global Optimization Toolbox, and with the *gamultiobj* algorithm, it is possible to find a Pareto Front.

In our case, however, we can not do that for two reasons:

1. it is not possible to give as input a non-linear constraint;

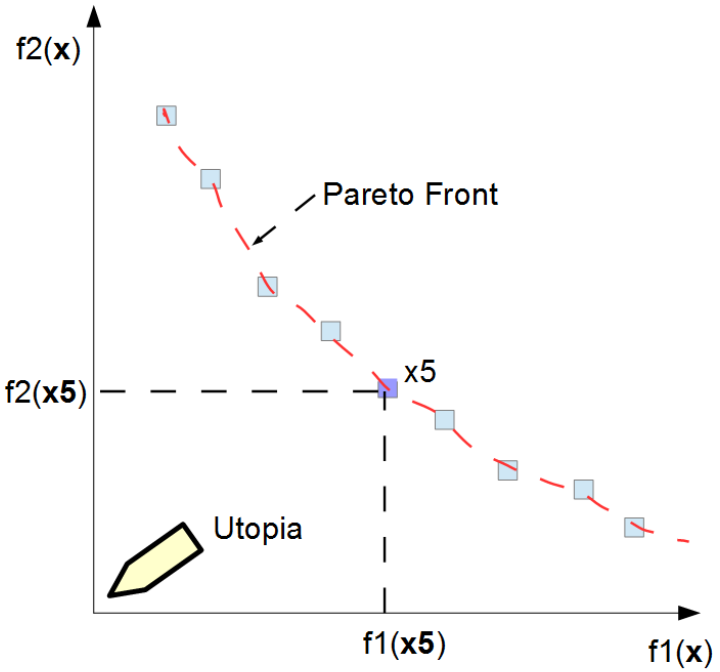

Figure B.1: Example of Pareto Front.

2. since we are not considering the thermal dissipation of the losses, the minimum volume and the minimal losses are achieved with the smallest volume allowed. And since the linear inequalities conditions are set through a $\leq$ and not through a $<$, are seen as optimal solutions trivial ones.

Weighted Approach A method to find the optimal values that minimize two or more functions is the *weighted sum method*. It is possible to find the minimum with a single objective algorithm of a function $F(x)$, that is the sum of all the objective functions, weighted with coefficients from 0 to 1.

$$\begin{cases} \min F(x) = \min \sum_{i=1}^{N} \alpha_i f_i(x),\ i = 1, \ldots, N; \\ \alpha_i \in [0,\ 1]; \\ \sum_{i=1}^{N} \alpha_i = 1. \end{cases} \tag{B.1}$$

Where N is the number of objectives. The values of α means the "importance" of a certain objective function respect to the others.

This approach ideally allows to find a Pareto Front with the single objective algorithm. It is possible then to set easily also non-linear constraints.

However, we do not use this method because the choice of the weighting coefficients is arbitrary, and it is not always possible to find a Pareto Front.

Bibliography

[1] China's rare earth dominance. Wikinvest, August 2010.

[2] China warns its rare earth reserves are declining. BBC news, June 2012.

[3] M. Andriollo, G. Martinelli, and A. Morini. *I trasformatori, teoria ed esercizi*. Libreria Cortina Padova, 2010.

[4] Nicola Bianchi. *Calcolo delle Macchine Elettriche col Metodo degli Elementi Finiti*. C.L.E.U.P., 2001.

[5] WM. Colone and T. McLyman. *Transformer and Inductor Design Handbook*. Marcel Dekker, Inc., 2004.

[6] ©2005 Fairchild Semiconductor Corporation. *FDP55N06/PDPF55N06*.

[7] ©2011 Diodes Incorporated. *MBR20100CTP*.

[8] ©Microchip Technology Inc. *SMPS AC/DC Reference Design User's Guide*, 2008.

[9] CEDRAT Flux®. *User's Guide*.

[10] S. Friedrich, G. Vivier et al. Design of a brushless rotor supply for a wound rotor synchronous machine for integrated starter generator. In *IEEE Vehicle Power and Propulsion Conference*, pages 236–241, 2007.

[11] E. Illano. Separately excited synchronous motor as high efficient drive in electric vehicles. *ATZ elektronik*, 8:44 – 49, 2013.

[12] E. Illano et al. E-machine with inductive energy transfer. *ATZ elektronik*, 8:20–24, 2013.

[13] Texas Instruments. Phase-shifted full-bridge, zero-voltage transition design considerations. Technical report, Texas Instruments Application Report, 2011.

[14] J. Legrangerl et al. Comparison of two optimal rotary transformer designs for highly constrained applications. In *IEMDC '07*, volume 2, pages 1546–1551, 2007.

[15] Magnetics®. *T Material datasheet*.

[16] Mathworks MATLAB®. *User's Guide*. The MathWorks, Inc.

[17] Ned Mohan, Tore M. Undeland, and William P. Robbins. *Elettronica di potenza*. Hoepli, 2003.

[18] Konstantinos D. Papastergiou and D. E. Macpherson. Contact-less transfer of energy by means of a rotating transformer. In *ISIE 2005 - IEEE International Symposium on Industrial Electronics*, volume 4, pages 1735–1740, 2005.

[19] Peter P. Poworoznek. http://www.ewp.rpi.edu/hartford/users/papers/engr/ernesto/poworp/project/4.%20supporting_material/books/32669_04.pdf.

[20] REUTERS. Canadian firms step up search for rare-earth metals. The New York Times, September 2009.

[21] Walter Schmidt. http://schmidt-walter.eit.h-da.de/smps_e/vgw_smps_e.html.

[22] J.P.C. Smeets et al. Comparison of winding topologies in a pot core rotating transformer. In *Optimization of Electrical and Electronic Equipment (OPTIM)*, 2010.

[23] J.P.C. Smeets et al. Optimal design of a pot core rotating transformer. In *IEEE Energy Conversion Congress and Exposition*, 2010.

[24] E. C. Snelling. *Soft Ferrites*. Iliffe Books, 1969.